

SPECIFICATION-GUIDED TEMPORAL LOGIC CONTROL FOR STOCHASTIC SYSTEMS: A MULTI-LAYERED APPROACH

BIRGIT C. VAN HUIJGEVOORT, RUOHAN WANG,
SADEGH SOUDJANI AND SOFIE HAESAERT*

Abstract. Designing controllers to satisfy temporal requirements has proven to be challenging for dynamical systems that are affected by uncertainty. This is mainly due to the states evolving in a continuous uncountable space, the stochastic evolution of the states, and infinite-horizon temporal requirements on the system evolution, all of which makes closed-form solutions generally inaccessible. A promising approach for designing provably correct controllers on such systems is to utilize the concept of *abstraction*, which is based on building simplified abstract models that can be used to approximate optimal controllers with provable closeness guarantees. The available abstraction-based methods are further divided into *discretization-based* approaches that build a finite abstract model by discretizing the continuous space of the system, and *discretization-free* approaches that work directly on the continuous state space without the need for building a finite space.

To reduce the conservatism in the sub-optimality of the designed controller originating from the abstraction step, this paper develops an approach that naturally has the flexibility to combine different abstraction techniques from the aforementioned classes and to combine the same abstraction technique with different parameters. First, we develop a *multi-layered* discretization-based approach with variable precision by combining abstraction layers with different precision parameters. Then, we exploit the advantages of both classes of abstraction-based methods by extending this multi-layered approach guided by the specification to combinations of layers with respectively discretization-based and discretization-free abstractions. We achieve an efficient implementation that is less conservative and improves the computation time and memory usage. We illustrate the benefits of the proposed multi-layered approach on several case studies.

1. Introduction. Stochastic difference equations are often used to model the behavior of complex systems that are operating in an uncertain environment, such as autonomous vehicles, airplanes, and drones. In this work, we are interested in automatically designing controllers with which we can give guarantees on the functionality of the controlled stochastic systems with respect to temporal logic specifications. Such automated control synthesis is often referred to as *correct-by-design* control synthesis [38, 7].

The techniques in correct-by-design synthesis are divided into two classes: methods that construct a finite-state abstraction of the original continuous-state model by discretizing the state space [7, 27], and methods that do not rely on a space discretization [46, 25]. The former is referred to as *discretization-based* techniques and the latter as *discretization-free* techniques. Selection of a synthesis technique from these classes depends on multiple factors including the complexity of the dynamics, the distribution of the uncertainty, the desired specification, and the labeling function defined on the state space of the system. Any of these techniques also have their own hyper-parameters that result in different computational complexities and different levels of conservatisms in the computed probability of satisfying the satisfaction. These hyper-parameters include among others the diameter of the discretization grid [35], confidence values for sampling-based computations [46], and the number of basis

*This work is supported by the Dutch NWO Veni project CODEC (18244) and the Horizon Europe EIC project SymAware (101070802). R. Wang and S. Haesaert are with the Department of Electrical Engineering, TU Eindhoven, The Netherlands. B. C. van Huijgevoort and S. Soudjani are currently with the Max Planck Institute for software systems. Part of the research was done when B. C. van Huijgevoort was with TU Eindhoven, The Netherlands. Emails: {[r.wang2](mailto:r.wang2@tue.nl), [s.Haesaert](mailto:s.Haesaert@tue.nl)}@tue.nl, {[bhuijgevoort,sadegh](mailto:bhuijgevoort,sadegh@mpi-sws.org)}@mpi-sws.org. A subset of the results of this manuscript has been presented as a conference paper entitled “Multi-layered simulation relations for linear stochastic systems” published by the IEEE 2021 European Control Conference (ECC).

functions [25]. A comparison between the current tools handling correct-by-design synthesis of stochastic systems applied to a set of standard benchmarks can be found in the ARCH competition reports [2, 1, 3].

As an example, consider a reach-avoid specification as illustrated in Fig. 1.1, where the objective is to avoid the red area and reach the green area from an arbitrary initial point $x(0)$ in the configuration space expressed in LTL as $\neg RED \cup GREEN$. We are interested in synthesizing a controller, or even simpler, planning a path that satisfies this specification subject to the dynamics of a given system. Since the dynamics of the system are influenced by uncertainty, the objective is to maximize the probability of satisfying this specification, referred to as the *satisfaction probability*. In certain circumstances, the satisfaction probability can be computed accurately by constructing a nominal path surrounded by a tube containing possible paths with a high probability, as is common with discretization-free approaches [46]. Such circumstances are for example 1) the distribution associated with the uncertainty has a small standard deviation, or 2) a large state space with a small avoid region and a large goal region that is far away from the avoid region. The accuracy of the approximated satisfaction probability can be improved by extending the usage of a single nominal path to sampling multiple paths in the state space. Still, such sampling-based approaches are only suitable for the circumstances mentioned before, and lack the accuracy to handle more challenging scenarios.

Discretization-based approaches such as [11, 12, 37] overcome the aforementioned limitation by (often manually) refining the grid until the accuracy of the satisfaction probability is sufficient. However, in practice, they are limited by the available memory and computation time. Put differently, when the available memory is limited, large-scale systems pose enormous challenges for discretization-based approaches, and discretization-free approaches are the only option. In this paper, we are interested in integrating these techniques and developing a *specification-guided* approach that naturally switches between and combines different techniques. More specifically, the approach employs a discretization-free technique whenever it gives acceptable accuracy and uses a discretization-based technique only when necessary, thereby effectively integrating the techniques to compute a single approximate satisfaction probability. The choice of the technique is determined by the specification, hence we refer to our approach as *specification-guided*.

Integrating both abstraction techniques while maintaining the theoretical guarantees is challenging and involves multiple alterations to the current results. A major challenge is the fact that these techniques often have different precisions. Therefore, we initially leave the integration of different abstraction techniques aside and focus on integrating discretization-based techniques that are utilizing approximate simulation

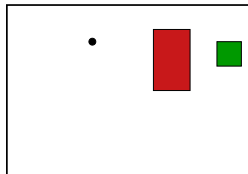


Fig. 1.1: Example of an output space for a reach-avoid specification. The red area is the area to avoid, the green area is the goal region, and the black dot is the initial state $x(0)$.

relations with different precisions. More specifically, we extend upon the preliminary results in [42] and switch between different layers each containing its own simulation relation with specific precision parameters. This is referred to as a *multi-layered approach* with homogeneous layers. Next, we propose a multi-layered methodology to feature layers with different abstraction techniques that are discretization-based or discretization-free, referred to as a multi-layered approach with heterogeneous layers.

1.1. Related Works. In the area of discretization-based techniques, multiple methods are related to variable precision through non-uniform partitioning of the state space. For deterministic systems, there exist methods that construct a non-uniform discretization grid [33, 39]. More specifically, they give an approximate bisimulation relation for variable precision (or dynamic) quantization and develop a method to locally refine a coarse finite-state abstraction based on the system dynamics. Furthermore, for deterministic systems, there also exist methods known as multi-layered discretization-based control synthesis. They focus on maintaining multiple finite-state abstraction layers with different precision, where they use the coarsest finite-state abstraction when possible [9, 10, 20, 24]. For stochastic models, non-uniform partitioning of the state space has been introduced for the purpose of verification [36] and for verification and control synthesis in the software tools FAUST² [37] and StocHy [11, 12]. Recent tools developments have considered utilizing interval Markov decision processes [29, 47]. In this paper, we consider approximate simulation relations that are used to quantify the similarity between a continuous-state model and its finite-state abstraction [23, 22]. Hence, we go beyond non-uniform partitioning and achieve a variable precision differently by allowing abstract models builds from both model order reduction methods and discretization of a reduced space.

Among the array of discretization-free techniques available, including control barrier certificate (CBC) [32] and stochastic model predictive control (SMPC) [15, 28, 30, 31], we emphasize the sampling-based approach [21, 45] for its exceptional relevance in our context. CBC seeks to delineate a barrier certificate level set to separate unsafe regions from system trajectories, offering a formal probabilistic safety certificate. Recent works on CBC applied to stochastic systems can be found for example in [14, 25, 34]. SMPC relies on iteratively solving constrained optimizations with most of the SMPC approaches handling safety requirements. Recent SMPC methods handles more expressive (finite-horizon) temporal specifications but still require solving stochastic optimizations that are computationally expensive [17, 18]. In contrast, the sampling-based approach used in this paper presents a distinct advantage by enabling the construction of Probabilistic Roadmaps (PRMs), a versatile tool both for navigating the complexities of stochastic systems, as well as for the integration with dynamic programming technique, which is the core method we use for obtaining the control policy. A sampling-based approach helps to lift the exponential computational complexity from the space discretization, a.k.a. *curse of dimensionality*, by treating a complex problem using random sampling to approximate the solution. The simplicity of implementing a sampling-based approach motivates us to choose it as the discretization-free method in this paper.

1.2. Contributions. We consider abstraction techniques based on approximate simulation relations that allow both model-order reduction and space discretization with quantification of the approximation errors. We start with allowing variable precision by presenting a simulation relation that contains multiple precision layers. For such relations, we develop an algorithm to determine a switching strategy and a robust dynamic programming approach such that we can compute a lower bound on

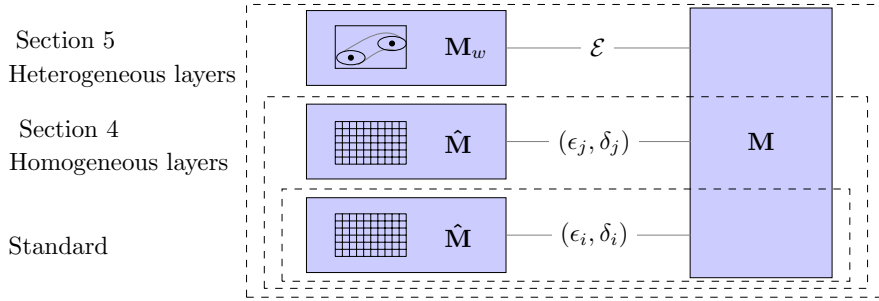


Fig. 1.2: Overview of the structure of this paper with the homogeneous-layered approach (two bottom layers) in Section 4 and the heterogeneous-layered approach (all layers) in Section 5. Precision ϵ_i , \mathcal{E} stand for output deviations, and δ_i stands for the probabilistic deviations [42].

the probability of satisfying the given specification. We then extend the developed multi-layered methodology to allow for layers with a discretization-free technique and layers with a discretization-based technique, therefore, improving the efficiency and scalability of our method. To this end, we implement a discretization-free technique that constructs a graph based on samples of the state space. The different approaches discussed in this paper are graphically illustrated in Fig. 1.2. More specifically, the approach of this paper has the following contributions.

- **Homogeneous layers.** First, we introduce a multi-layered approach with variable precision. Here, we use multiple homogeneous layers, in which *one finite-state model* with multiple layers and *multiple similarity quantifications* is used. We quantify the similarity compared to the original model with different deviation bounds in the output map (ϵ) and in the transition probabilities (δ). By doing so, we achieve a multi-layered simulation relation with variable precision. To perform the value iteration, we modify the standard dynamic programming (DP) operator, such that it suits this multi-layered approach.
- **Heterogeneous layers.** Then, we combine the multi-layered approach with a model that is constructed using a discretization-free technique. Hence, we use different abstract models. To perform the value iteration with heterogeneous layers, we integrate the DP operator of the discretization-free layer with the DP operator of the multi-layered approach with homogeneous layers.

A subset of the results of this paper is presented in [41]. This paper substantially expands the preliminary results of [41] in the following directions: (a) Different abstraction techniques are integrated into the proposed approach; (b) The underlying dynamic programming computations are adapted to allow this integration; (c) A heuristic approach to derive an optimal switch strategy is included; (d) Implementation of case studies is expanded and enriched by incorporating more complex and higher-dimensional scenarios, thereby providing a more comprehensive and robust analysis; and (e) The proofs of statements are provided.

1.3. Overview. The main part of this paper is structured as illustrated in Fig. 1.2. The structure of this paper is as follows. In Section 2, we discuss the considered model and specifications, and formulate the problem statement for a general class of nonlinear stochastic difference equations. In Section 3, we motivate the need

for a multi-layered approach by applying a discretization-based and discretization-free approach to a specific example and evaluating the results. Besides that, we give high level details of the abstract models and similarity quantification. In Section 4, we discuss the multi-layered approach with homogeneous layers. More precisely, we achieve variable precision by having multiple precision parameters for a single abstract model. In Section 5, we extend the multi-layered method to allow discretization-free layers and discretization-based layers resulting in a heterogeneous approach. Finally, in Section 6, we apply our method to multiple case studies. We end this paper with a conclusion.

2. Problem formulation. Notation. We limit ourselves to spaces that are finite, Euclidean, or Polish. The Borel measurable space of a set $\mathbb{X} \subset \mathbb{R}^n$ is denoted by $(\mathbb{X}, \mathcal{B}(\mathbb{X}))$ with $\mathcal{B}(\mathbb{X})$ being the Borel sigma-algebra on \mathbb{X} . A probability measure \mathbb{P} over this space has realization $x \sim \mathbb{P}$, with $x \in \mathbb{X}$. Furthermore, a time update of a state variable x is interchangeably denoted by $x(t+1)$, x_{t+1} or x^+ .

Model. We consider general Markov decision processes (gMDP) as defined in [23, 22] as follows.

DEFINITION 2.1 (general Markov decision process (gMDP)). *A gMDP is a tuple $\mathbf{M} = (\mathbb{X}, x_0, \mathbb{U}, \mathbf{t}, \mathbb{Y}, h)$ with state space \mathbb{X} , initial state $x_0 \in \mathbb{X}$, input space \mathbb{U} , and with output space \mathbb{Y} and measurable output map $h : \mathbb{X} \rightarrow \mathbb{Y}$. The transitions kernel $\mathbf{t} : \mathbb{X} \times \mathbb{U} \times \mathcal{B}(\mathbb{X}) \rightarrow [0, 1]$ assigns to each state $x \in \mathbb{X}$ and input $u \in \mathbb{U}$ a probability measure $\mathbf{t}(\cdot | x, u)$ over $(\mathbb{X}, \mathcal{B}(\mathbb{X}))$.*

We consider output space \mathbb{Y} to be a metric space and denote the class of all models with the same metric output space $(\mathbb{Y}, \mathbf{d}_{\mathbb{Y}})$ as $\mathcal{M}_{\mathbb{Y}}$. The behavior of a gMDP with n_x -dimensional state space $\mathbb{X} \subset \mathbb{R}^{n_x}$ can equivalently be described by a stochastic difference equation. We consider discrete-time systems whose dynamics are described by a stochastic difference equation with Gaussian disturbance

$$(2.1) \quad \mathbf{M} : \begin{cases} x(t+1) = f(x(t), u(t), w(t)) \\ y(t) = h(x(t)), \quad \forall t \in \{0, 1, 2, \dots\}, \end{cases}$$

with state $x(t) \in \mathbb{X}$, input $u(t) \in \mathbb{U}$, disturbance $w(t) \in \mathbb{W} \subseteq \mathbb{R}^{n_w}$, output $y(t) \in \mathbb{Y}$, and with measurable functions $f : \mathbb{X} \times \mathbb{U} \times \mathbb{W} \rightarrow \mathbb{X}$ and $h : \mathbb{X} \rightarrow \mathbb{Y}$. The system is initialized with $x(0) = x_0 \in \mathbb{X}$, and $w(t)$ is an independently and identically distributed sequence with realizations $w \sim \mathbb{P}_w = \mathcal{N}(\mu, \Sigma)$.

A finite path of the model (2.1) is a sequence $\omega_{[0,t]} := x_0, u_0, x_1, u_1, \dots, x_t$. An infinite path is a sequence $\omega := x_0, u_0, \dots$. The paths start at $x_0 = x(0)$ and are built up from realizations $x_{t+1} = x(t+1)$ based on (2.1) given a state $x(t) = x_t$, input $u(t) = u_t$ and disturbance $w(t)$ for each time step t . We denote the state trajectories as $\mathbf{x} = x_0, x_1, \dots$, with associated suffix $\mathbf{x}_t = x_t, x_{t+1}, \dots$. The output y_t contains the variables of interest for the performance of the system and for each state trajectory, there exists a corresponding output trajectory $\mathbf{y} = y_0, y_1, \dots$, with associated suffix $\mathbf{y}_t = y_t, y_{t+1}, \dots$.

A control strategy is a sequence $\boldsymbol{\mu} = (\mu_0, \mu_1, \mu_2, \dots)$ of maps $\mu_t(\omega_{[0,t]}) \in \mathbb{U}$ that assigns for each finite path $\omega_{[0,t]}$ an input $u(t) = u_t$. The control strategy is a Markov policy if μ_t only depends on x_t , that is $\mu_t : \mathbb{X} \rightarrow \mathbb{U}$. We refer to a Markov policy as *stationary* if μ_t does not depend on the time index t , that is $\boldsymbol{\mu} = (\mu, \mu, \dots)$ for some μ . In this work, we are interested in control strategies denoted as \mathbf{C} that can be represented with finite memory, that is, policies that are either time-stationary Markov policies or have finite internal memory. A policy with finite internal memory

first maps the finite state execution of the system to a finite set (memory), followed by computing the input as a function of the system state and the memory state. By doing so, we can satisfy temporal specifications on the system trajectories.

Specifications. To express (unbounded time-horizon) temporal logic specifications, we use the syntactically co-safe linear temporal logic specifications (scLTL) [7, 26]. Consider atomic propositions p_1, p_2, \dots, p_N that are true or false. The set of atomic propositions and the corresponding alphabet are denoted by $\text{AP} = \{p_1, \dots, p_N\}$ and 2^{AP} , respectively. Each letter $\pi \in 2^{\text{AP}}$ contains the set of atomic propositions that are true. A (possibly infinite) string of letters forms a word $\boldsymbol{\pi} = \pi_0, \pi_1, \dots$, with associated suffix $\boldsymbol{\pi}_t = \pi_t, \pi_{t+1}, \dots$. The output trajectory $\mathbf{y} = y_0, y_1, \dots$ of a system (2.1) is mapped to the word $\boldsymbol{\pi} = L(y_0), L(y_1), \dots$ using labeling function $L : \mathbb{Y} \rightarrow 2^{\text{AP}}$ that translates each output to a specific letter $\pi_t = L(y_t)$. Similarly, suffixes \mathbf{y}_t are translated to suffix words $\boldsymbol{\pi}_t$. By combining atomic propositions with logical operators, the language of scLTL can be defined as follows.

DEFINITION 2.2 (scLTL syntax). *An scLTL formula ϕ over a set of atomic propositions AP , with $p \in \text{AP}$ has syntax*

$$(2.2) \quad \phi ::= p \mid \neg p \mid \phi_1 \wedge \phi_2 \mid \phi_1 \vee \phi_2 \mid \bigcirc \phi \mid \phi_1 \mathbf{U} \phi_2.$$

The semantics of this syntax can be given for the suffixes $\boldsymbol{\pi}_t$. An atomic proposition $\boldsymbol{\pi}_t \models p$ holds if $p \in \boldsymbol{\pi}_t$, while a negation $\boldsymbol{\pi}_t \models \neg \phi$ holds if $\boldsymbol{\pi}_t \not\models \phi$. Furthermore, a conjunction $\boldsymbol{\pi}_t \models \phi_1 \wedge \phi_2$ holds if both $\boldsymbol{\pi}_t \models \phi_1$ and $\boldsymbol{\pi}_t \models \phi_2$ are true, while a disjunction $\boldsymbol{\pi}_t \models \phi_1 \vee \phi_2$ holds if either $\boldsymbol{\pi}_t \models \phi_1$ or $\boldsymbol{\pi}_t \models \phi_2$ is true. Also, a next statement $\boldsymbol{\pi}_t \models \bigcirc \phi$ holds if $\boldsymbol{\pi}_{t+1} \models \phi$. Finally, an until statement $\boldsymbol{\pi}_t \models \phi_1 \mathbf{U} \phi_2$ holds if there exists an $i \in \mathbb{N}$ such that $\boldsymbol{\pi}_{t+i} \models \phi_2$ and for all $j \in \mathbb{N}, 0 \leq j < i$, we have $\boldsymbol{\pi}_{t+j} \models \phi_1$. A system satisfies a specification if the generated word $\boldsymbol{\pi}_0 = L(\mathbf{y}_0)$ satisfies the specification, i.e., $\boldsymbol{\pi}_0 \models \phi$.

For control synthesis purposes, an scLTL specification can be written as a deterministic finite-state automaton (DFA), defined by the tuple $\mathcal{A} = (Q, q_0, \Sigma_{\mathcal{A}}, \tau_{\mathcal{A}}, Q_f)$. Here, Q , q_0 , and Q_f denote the set of states, initial state, and set of accepting states, respectively. Furthermore, $\Sigma_{\mathcal{A}} = 2^{\text{AP}}$ denotes the input alphabet and $\tau_{\mathcal{A}} : Q \times \Sigma_{\mathcal{A}} \rightarrow Q$ is a transition function. For any scLTL specification ϕ , there exists a corresponding DFA \mathcal{A}_{ϕ} such that the word $\boldsymbol{\pi}$ satisfies this specification $\boldsymbol{\pi} \models \phi$, iff $\boldsymbol{\pi}$ is accepted by \mathcal{A}_{ϕ} . Here, acceptance by a DFA means that there exists a trajectory $q_0 q_1 q_2 \dots q_f$, that starts with q_0 , evolves according to $q_{t+1} = \tau_{\mathcal{A}}(q_t, \boldsymbol{\pi}_t)$, and ends at $q_f \in Q_f$.

Correct-by-design control synthesis focuses on designing a controller \mathbf{C} , for model \mathbf{M} and specification ϕ , such that the controlled system $\mathbf{M} \times \mathbf{C}$ satisfies the specification, denoted as $\mathbf{M} \times \mathbf{C} \models \phi$. For stochastic systems, we are interested in the satisfaction probability, denoted as $\mathbb{P}(\mathbf{M} \times \mathbf{C} \models \phi)$. The general problem considered in this paper is the following.

Problem. Given model \mathbf{M} as in (2.1), an scLTL specification ϕ , and a probability $p_{\phi} \in [0, 1]$, find a controller \mathbf{C} , such that

$$(2.3) \quad \mathbb{P}(\mathbf{M} \times \mathbf{C} \models \phi) \geq p_{\phi}.$$

3. Motivation for a multi-layered approach. In this section, we justify the need for a multi-layered approach with the help of a running example. We first introduce the running example, followed by discussions on discretization-based (DB) techniques and discretization-free (DF) techniques, respectively. Then, we compare the results of applying standard DB and DF approaches on the running example, and

summarize their merits and drawbacks. We conclude the section by emphasizing the need for a multi-layered approach.

Running example (specification and dynamics). As a running example, we consider a scLTL-specified scenario that we will refer to as the package delivery scenario. For this scenario, we consider multiple regions defined on the output space \mathbb{Y} , namely a pick-up region $P_1 = [-4, -3]^2$, a delivery region $P_3 = [3, 5] \times [-2, -0.5]$, a strict avoid region $P_4 = [0, 1] \times [-4, 0]$, and a region where we lose a package $P_2 = [0, 1] \times [0, 2.5]$. The goal of the controller is to make sure that a package is picked up at P_1 and delivered to P_3 while avoiding P_4 . Region P_2 is fine to visit without a package, but once crossed while carrying a package, the package is lost and a new package has to be picked up from P_1 . We label the regions P_1, P_3, P_4 and P_2 as p_1, p_3, p_4, p_2 respectively. The specification of the scenario is written in scLTL as

$$(3.1) \quad \phi_{PD} = \neg p_4 \text{ U } (p_1 \wedge (\neg(p_4 \vee p_2) \text{ U } p_3)).$$

The associated DFA is given in Fig. 3.1.

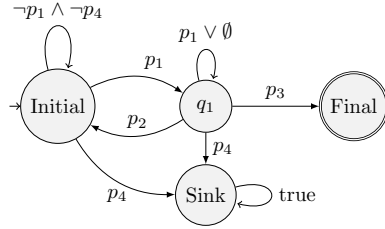


Fig. 3.1: Cyclic DFA corresponding to the specification of the package delivery. Here, \emptyset denotes the *empty set*, which means that all atomic propositions $p \in \text{AP}$ are false.

The dynamics of the robot carrying the package is a 2-dimensional linear system, as in (2.1):

$$(3.2) \quad \mathbf{M} : \begin{cases} x(t+1) = 0.9I_2x(t) + 0.5I_2u(t) + \sqrt{0.25}I_2w(t) \\ y(t) = I_2x(t), \quad \forall t \in \{0, 1, 2, \dots\}, \end{cases}$$

with states $x \in \mathbb{X} = [-20, 5]^2$, inputs $u \in \mathbb{U} = [-5, 5]^2$, outputs $y \in \mathbb{Y} = \mathbb{X}$ and Gaussian disturbance $w(t) \sim \mathcal{N}(\mathbf{0}, I_2)$.

3.1. Discretization-based method. For continuous-state stochastic models, it is computationally hard to design a controller \mathbf{C} and compute the satisfaction probability $\mathbb{P}(\mathbf{M} \times \mathbf{C} \models \phi)$ [4]. We adopt the common solution in correct-by-design control synthesis which is to approximate the continuous-state model by a finite-state version. This step is often called *abstraction*, and we perform it by partitioning or discretization of the state space as in [22].

Model. Suppose that we have approximated the continuous-state model as given in (2.1), with the following abstract model

$$(3.3) \quad \hat{\mathbf{M}} : \begin{cases} \hat{x}(t+1) = \hat{f}(\hat{x}(t), \hat{u}(t), \hat{w}(t)) \\ \hat{y}(t) = \hat{h}(\hat{x}(t)), \end{cases}$$

with state $\hat{x} \in \hat{\mathbb{X}}$ being in a finite space $\hat{\mathbb{X}}$, initialized at $\hat{x}(0) = \hat{x}_0$ and with input $\hat{u} \in \hat{\mathbb{U}}$, output $\hat{y} \in \mathbb{Y}$ and disturbance $\hat{w} \in \hat{\mathbb{W}}$. Furthermore, we have functions

$\hat{f} : \hat{\mathbb{X}} \times \hat{\mathbb{U}} \times \hat{\mathbb{W}} \rightarrow \hat{\mathbb{X}}$ and $\hat{h} : \hat{\mathbb{X}} \rightarrow \mathbb{Y}$, and $\hat{w}(t)$ is an independently and identically distributed sequence with realizations $\hat{w} \sim \mathbb{P}_{\hat{w}}$. Beyond the given representative points, one generally adds a sink state to both the continuous- and the finite-state model to capture transitions that leave the bounded set of states.

Similarity quantification. We use the abstract model in (3.3) to compute a lower bound on the probability of satisfying specification ϕ . To preserve this lower bound, we need to quantify the similarity between the models (2.1) and (3.3). We consider an approximate simulation relation as in Def. 4 in [42], since this is suitable for scLTL, which can be unbounded in time. This method for quantifying the similarity is based on an explicit coupling between the models (2.1) and (3.3), which allows for analyzing how close the probability transitions are. Def. 4 in [42] is based on the following observation. Given a simulation relation $\mathcal{R} \subset \hat{\mathbb{X}} \times \mathbb{X}$, for all pair of states inside this relation $(\hat{x}, x) \in \mathcal{R}$, and for all inputs $\hat{u} \in \hat{\mathbb{U}}$ we can quantify a lower bound on the probability that the next pair of states is also inside this simulation relation, i.e. $(\hat{x}^+, x^+) \in \mathcal{R}$. Hence, for all states $(\hat{x}, x) \in \mathcal{R}$, $\forall \hat{u} \in \hat{\mathbb{U}}$, we require that

$$(3.4) \quad (\hat{x}^+, x^+) \in \mathcal{R}$$

has a lower bound on its probability denoted by $1 - \delta$ under the transitions in the coupled model.

The approximate simulation relation in [42, Def. 4] does not only quantify the similarity based on the probability deviation δ but also on output deviation ϵ . Furthermore, if $\hat{\mathbf{M}}$ is (ϵ, δ) -stochastically simulated by \mathbf{M} , then this is denoted as $\hat{\mathbf{M}} \preceq_{\epsilon}^{\delta} \mathbf{M}$. In [42], it has been shown that ϵ and δ have a trade-off. Increasing ϵ decreases the achievable δ and vice versa. To compute the deviation bounds (ϵ, δ) , an optimization problem constrained by a set of parameterized matrix inequalities is given in [42].

Running example (similarity quantification for DB approaches). To apply a DB approach, we first construct a finite-state abstraction in the form of $\hat{\mathbf{M}}$ (3.3) by gridding the state space \mathbb{X} of \mathbf{M} in (3.2) with 568×563 grid cells and the input space \mathbb{U} with 14×14 grid cells. Details on constructing such an abstraction can be found in [42, Sec. 4]. To compute the satisfaction probability we have to quantify the similarity. To this end, we choose the interface function $u = \hat{u}$ and relation $\mathcal{R} = \{(\hat{x}, x) \in \hat{\mathbb{X}} \times \mathbb{X} \mid \|x - \hat{x}\|_D \leq \epsilon\}$, with $\epsilon = 0.18$ and D a symmetric positive definite weighting matrix. Next, we obtain the approximate simulation relation between the original model \mathbf{M} (3.2) and its finite-state abstraction in the form of $\hat{\mathbf{M}}$ (3.3) as $(\epsilon, \delta) = (0.18, 0.1217)$ and $D = I_2$ using SySCoRe tool [43] based on linear matrix inequalities as in [42].

3.2. Discretization-free method. Model and similarity quantification.

For the DF method, we consider an approximate relation similar to the one in DB method, to quantify the similarity between our abstract model of the DF layer and the model (2.1). The reason we emphasize the similarity quantification here is that the output deviation ϵ , i.e. ϵ_w is encoded in the model construction. Consider a finite set of states taken from the state space of the original model \mathbf{M} as in (2.1), that is $x_w \in \mathbb{X}_w \subset \mathbb{X}$, referred to as waypoints. We associate to each waypoint an ellipsoid

$$(3.5) \quad \mathcal{E}(x_w) := \{x \in \mathbb{X} \mid \|x - x_w\|_{D_w} \leq \epsilon_w\}$$

that contains the states $x \in \mathbb{X}$ of the original model. Here, D_w is a symmetric positive definite matrix. Note that the center of \mathcal{E} equals x_w , but without loss of generality, we consider its shape the same for all $x_w \in \mathbb{X}_w$. We now define a state transition function

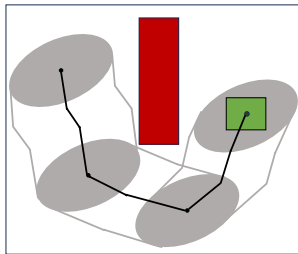


Fig. 3.2: Example of a state trajectory (black line) of a waypoint model with the corresponding tube in gray. The red and green regions are respectively an avoid and a goal region projected from the output space to the state space. The black dots are the waypoints x_w and the gray ellipsoids are the sets \mathcal{E} . Note that this waypoint model is not well-posed since not all of the outputs corresponding to the top right ellipsoid have the same label.

$\Delta_w : \mathbb{X}_w \times \mathbb{X}_w \rightarrow [0, 1]$ that gives a lower bound on the probability of reaching waypoint x'_w in a finite number of steps n_s . More specifically, for all $x_w \in \mathcal{E}(x_w)$ there exists a sequence of control strategies, such that with a probability of at least $\Delta_w(x_w, x'_w)$, $\exists n_s \in \mathbb{N}$, such that $x_{k+n_s} \in \mathcal{E}(x'_w)$. Together, this allows us to define the following waypoint model

$$(3.6) \quad \mathbf{M}_w = (\mathbb{X}_w, x_{w,0}, \Delta_w, \mathbb{Y}, h_w),$$

with initial state $x_{w,0} \in \mathbb{X}_w$, outputs $y_w \in \mathbb{Y}$, and output map $h_w : \mathbb{X}_w \rightarrow \mathbb{Y}$.

Specification. To handle temporal logic specifications based on the model \mathbf{M}_w , we require that \mathbf{M}_w is well-posed with respect to labeling $L : \mathbb{Y} \rightarrow 2^{\text{AP}}$, if $\forall x_w \in \mathbb{X}_w$:

1. all outputs y corresponding to states $x \in \mathcal{E}(x_w)$ have the same label, and
2. the outputs corresponding to paths from x_w to x'_w either never change label or only once.

These two assumptions allow us to keep track of the DFA state in a simple manner, which is necessary when considering temporal logic specifications.

The construction of the waypoint model, allows us to handle specifications given using $\text{sLTL} \setminus \bigcirc$, where the \bigcirc -operator is excluded since the number of time steps between waypoints is usually larger than 1. An exemplary visualization of a waypoint model is given in Fig. 3.2.

Available methods. The construction of paths in the waypoint model is in essence the same as solving a (deterministic) reach-avoid problem, for which a variety of methods are available [19, 5, 8]. For some situations, the transition probability Δ_w can even be computed directly via a continuous-state (stochastic) model using for example the tool `SReachTools` [46]. In this paper, we utilize a sampling-based approach to construct our model of the DF layer. By defining the layer in this manner, we can use dynamic programming (as defined later in this paper) to make a connection between DB and DF methods.

Running example (similarity quantification for DF approaches). To apply the DF approach, we first construct a waypoint model in the form of \mathbf{M}_w (3.6). To this end, we uniformly sample well-posed points in the state space for initializing a directed graph. Vertices and edges of the graph respectively correspond to states $x \in \mathcal{E}(x_w)$, and possible transitions of $x_w \rightarrow x'_w$. The approach is summarized in Alg. 3.1. We

Algorithm 3.1 Construct waypoint model

- 1: **Input:** \mathbf{M}
 - 2: $\hat{\mathbb{X}}_s \leftarrow$ Uniformly sample well-posed points of \mathbb{X}
 - 3: $\mathcal{G}_{\text{PRM}} \leftarrow$ Construct a directed graph with waypoints $x_w \in \hat{\mathbb{X}}_s$ and well-posed edges based on \mathbf{M}
 - 4: **while** \mathcal{G}_{PRM} is not strongly connected **do**
 - 5: $\hat{\mathbb{X}}_s \leftarrow$ Uniformly sample and add new well-posed points of \mathbb{X}
 - 6: $\mathcal{G}_{\text{PRM}} \leftarrow$ Augment the graph with new well-posed edges
 - 7: **end while**
 - 8: Construct \mathbf{M}_w based on \mathcal{G}_{PRM}
 - 9: **Output:** \mathbf{M}_w
-

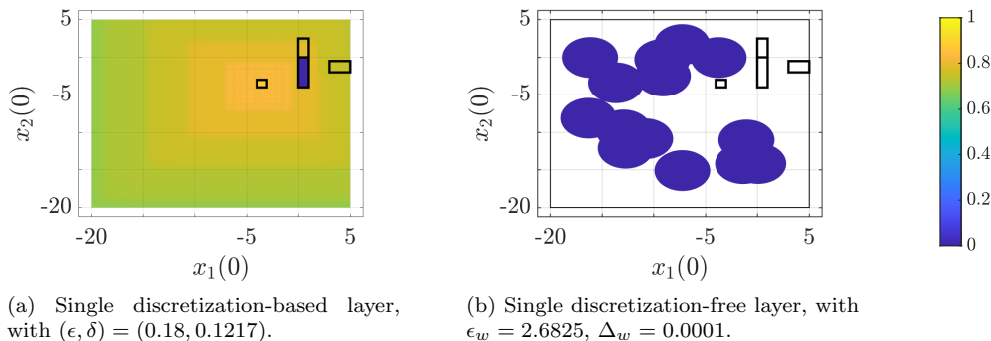


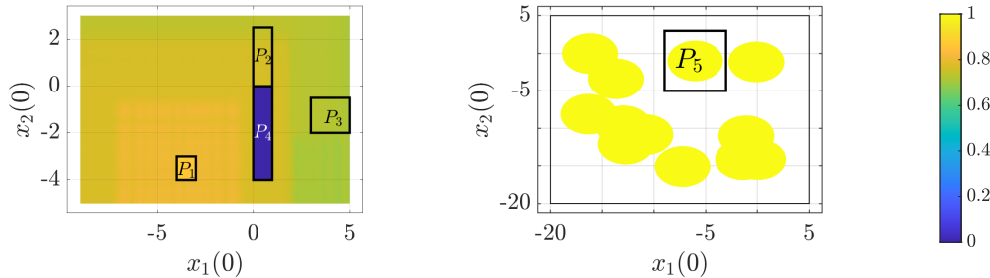
Fig. 3.3: Complete running example with state space $\mathbb{X} = [-20, 5]^2$. Robust satisfaction probabilities computed by applying a DB approach in (a), and by applying a DF approach in (b).

sample 48 waypoints in total for our running example and choose $n_s = 3$ for the number of steps between waypoints. To compute the satisfaction probability, we have to quantify the similarity. To this end, choose the lower bound of the transition probability $\Delta_w = 0.0001$. We compute the similarity quantification between the original model \mathbf{M} (3.2) and its waypoint model \mathbf{M}_w in the form of (3.6) for interface function $u = \hat{u}$, and obtain $\epsilon_w = 2.6825$. Details on this computation are given in Appendix B.

3.3. Analysis of the running example. In this subsection, we compare computation time, and memory usage, and analyze the robust satisfaction probabilities obtained using different approaches, i.e., the pure DB approach (one single DB layer) and the pure DF approach (one single DF layer). The results of applying those approaches to the running example are presented in Fig. 3.3. Here, the satisfaction probability is shown for the initial DFA state (labeled *Initial* in Fig. 3.1).

The average running time when applying the pure DB approach is 14.44 seconds, when applying the pure DF approach is 0.3442 seconds. The corresponding memory usage is equal to 2706 MB and 0.027 MB respectively.¹ Computational efficiency of

¹All simulations are performed on a computer with a 3.4 GHz 13th Gen Intel Core i7-13700K processor and 64 GB 3200 MHz memory.



(a) Single discretization-based layer, with $(\epsilon, \delta) = (0.18, 0.1217)$ for the smaller state space.

(b) Single discretization-free layer, with $\epsilon_w = 2.6825, \Delta_w = 0.0001$.

Fig. 3.4: Split-up, unconnected running example. Robust satisfaction probabilities computed by applying a DB approach to a specific part of the state space, that is $\mathbb{X}_{\text{small}} = [-9, 5] \times [-5, 3] \subset \mathbb{X}$ in (a), and by applying a DF approach to the complete state space $\mathbb{X} = [-20, 5]^2$ to reach the area $P_5 = [-9, -3] \times [-5, 3] \subset \mathbb{X}_{\text{small}}$ in (b).

the DF method, (sampling-based approach, in our case) is prominent. However, it can be observed that due to the nature of the pure DF method, in this specific case, for any well-posed waypoint model \mathbf{M}_w , the lower bounds on the satisfaction probabilities converge to zero after 3-5 iterations during dynamic programming, while following the DB method the lower bound is a lot higher. This DF approach is not accurate enough for this specific case. In our DF approach, due to the inherent trade-off between ϵ_w and Δ_w of our waypoint model \mathbf{M}_w , it is impossible to obtain nonzero satisfaction probabilities for our package delivery case. Intuitively, the regions p_1, \dots, p_4 are too small for a model with such a (relatively) large stochastic disturbance. Next, we will analyze the results of both approaches in more detail.

DB approach. In Fig. 3.3a, we can see that due to the specification of the running example, the satisfaction probabilities decrease the further you are from the region P_1 . In our running example, the satisfaction probabilities decrease rapidly due to the relatively large value of δ .

DF approach. To elaborate on the reasons causing the satisfaction probabilities to (and will always) be 0 when a DF approach is used, we consider two cases. The first case is to assume we tune Δ_w so that ϵ_w is small enough to make sure we have well-posed sample states inside our interested regions, i.e., P_1, P_2, P_3 , or P_4 . By making sure we sample sufficient amounts of well-posed sample states, our transition probability deviation Δ_w will be way too high consequently such that the robust satisfaction probabilities will drop to 0 after 1 or 2 control actions. The second case is that we maintain our transition probability deviation Δ_w sufficiently low, which is what we do to obtain the result in Fig. 3.3b. The consequence of this choice is that because our interested regions, i.e., P_1, P_2, P_3 , and P_4 are very small (compared to our ellipsoidal sets ϵ_w of our waypoint model), we will not be able to sample any well-posed states inside our interested regions, hence in terms of DFA, we are forever stuck in the beginning state q_0 and we obtained the trivial lowerbound of 0 on the satisfaction probability.

A multi-layered approach. Based on comparing the robust satisfaction proba-

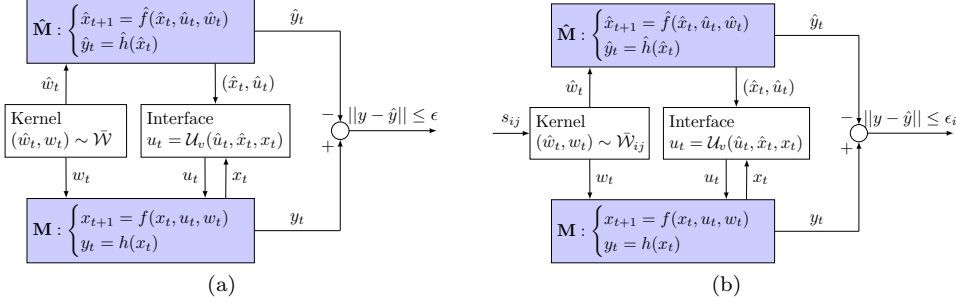


Fig. 3.5: Similarity quantification between the models \mathbf{M} and $\hat{\mathbf{M}}$. For a standard setting in (a) and for a multi-layered setting with homogeneous layers in (b).

bilities and computational efficiency between the DB approach and the DF approach, we conclude that DB approach exceeds DF approach in terms of accuracy, while DF approach surpasses DB approach in terms of efficiency. We, therefore, propose the heterogeneous approach through combining these two methods, to mitigate the drawbacks of applying two approaches separately and alone. To this end, we construct a DF layer for the complete state space and reduce the state space for which we construct the DB layer. By doing so, we exploit the accuracy of the DB approach around the area where the interested regions are clustered, and we exploit the computational efficiency of the DF approach for the “empty” area.

In this specific case, we would use the DB approach to grid the part of the state space $[-9, 5] \times [-5, 3]$, since this is where we need its accuracy. To handle the complete state space, we use the DF approach to reach this gridded part of the state space. To discover the potential benefit of combining a DB and a DF approach, we consider them separately next. First, we applied the DB approach using **SySCoRe** to the model (3.2) with state space $\mathbb{X} = [-9, 5] \times [-5, 3]$ by gridding the state space with 318×180 grid cells and the input space with 14×14 grid cells. We found $(\epsilon, \delta) = (0.18, 0.1217)$ and $D = I_2$ for the similarity quantification and obtained the satisfaction probability as in Fig. 3.4a. Next, we applied the DF approach to the model (3.2) with updated specification $\phi = \diamond p_5$, where p_5 corresponds to the region $P_5 = [-9, -3] \times [-5, 3]$. We obtained a waypoint model by sampling 48 well-posed points in \mathbb{X} and followed Alg. 3.1. We choose $\Delta_w = 0.0001$, which is much smaller than δ , to obtain a high satisfaction probability. We then compute $\epsilon_w = 2.6825$. The resulting robust satisfaction probability is given in Fig. 3.4b. Comparing these results to the original one in Fig. 3.3, we can conclude that indeed the DB approach works best for a small state space and can handle small labeled regions, while the DF approach works best for large state spaces with large labeled regions.

The overall goal of this paper is to combine these two results into one while maintaining guarantees on the lower bound of the satisfaction probability. We do this, by introducing different layers each containing its own abstraction approach. Throughout this paper, we use two running examples. The first running example, introduced in Section 3, will be used to illustrate our heterogeneous-layer approach. The second running example, referred to as *Running example A*, is a more complex variation of the first and will be used for the demonstration of the homogeneous-layer approach.

4. Homogeneous layers with variable precision. As mentioned before, we quantify the similarity between the original model \mathbf{M} (2.1) and abstract model $\hat{\mathbf{M}}$ (3.3) by using an approximate simulation relation as in Def. 4 in [42]. This notion is based on two deviation bounds; output deviation or precision ϵ , and probability deviation or confidence δ . The output deviation is graphically illustrated in Figure 3.5a. Here, we also see coupling between the two models \mathbf{M} and $\hat{\mathbf{M}}$ through a kernel and interface function as detailed in [42]. The probability deviation δ associated with the lower bound on the probability of (3.4) has an inverse variation relation with the output deviation ϵ . Intuitively, the probability that a pair of states remain in the same set is larger if the set itself is larger. In this setting, the (lower bound on the) probability is given by $1 - \delta$ and the set by simulation relation \mathcal{R} whose size is directly determined by ϵ . This indicates that a larger output deviation ϵ gives a smaller probability deviation δ . In the standard (single-layered) setting [42], only one (ϵ, δ) -pair is used to quantify the similarity between the two models \mathbf{M} and $\hat{\mathbf{M}}$, however, this (ϵ, δ) -pair is not unique.

In this section, we define a multi-layered simulation relation that allows variable precision using one abstract model, but different deviation bounds (ϵ, δ) . Furthermore, we detail an appropriate DP approach, discuss multiple computational improvements, and prove the control refinement.

4.1. Homogeneous-layered simulation relation. Current methods define one simulation relation for the whole state space, while we desire a multi-layered simulation relation $\mathcal{R} = \{\mathcal{R}_i\}$ with $i \in \{1, 2, \dots, N_R\}$ that switches between multiple simulation relations to allow for multiple (ϵ_i, δ_i) pairs, with $i \in \{1, 2, \dots, N_R\}$ where N_R denotes the number of simulation relations. Each simulation relation is denoted as \mathcal{R}_i and the corresponding precision as ϵ_i .

An example of a multi-layered simulation relation with two simulation relations is given in Fig. 4.1. Here, the self-loops represent remaining in the same simulation

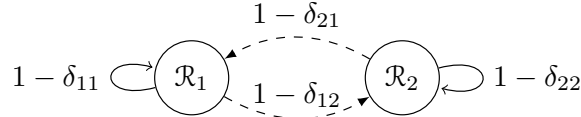


Fig. 4.1: Multi-layered simulation relation \mathcal{R} consisting of two simulation relations \mathcal{R}_1 and \mathcal{R}_2 . The edges are labeled with a lower bound on the probability that the transition occurs.

relation, and a switch is indicated by the dashed arrows. Similar to the invariance requirement in (3.4), we associate a lower bound on the probability of each transition from \mathcal{R}_i to \mathcal{R}_j as $1 - \delta_{ij}$, with $i, j \in \{1, 2, \dots, N_R\}$. Furthermore, we define ϵ , and δ with vector $\epsilon = [\epsilon_1, \epsilon_2, \dots, \epsilon_{N_R}]$, and matrix $\delta = [\delta_{ij}]_{ij}$. In the remainder of this paper, a switch from simulation relation \mathcal{R}_i to \mathcal{R}_j is denoted by the action s_{ij} , and we define the set of all possible switching actions by $\mathbb{S} := \{s_{ij} \text{ with } i, j \in \{1, 2, \dots, N_R\}\}$.

The similarity quantification between the two models is graphically represented in Fig. 3.5b and is based on coupling the transitions of the models. First, the control inputs u and \hat{u} are coupled through an interface function denoted by

$$(4.1) \quad \mathcal{U}_v : \hat{\mathbb{U}} \times \hat{\mathbb{X}} \times \mathbb{X} \rightarrow \mathbb{U}.$$

Next, the disturbances w and \hat{w} are coupled through a stochastic kernel $\bar{\mathcal{W}}_{ij}(\cdot|\hat{x}, x, \hat{u})$ in a similar fashion as in [42]. However, in this multi-layered setting, we compute multiple stochastic kernels $\bar{\mathcal{W}}_{ij}(\cdot|\hat{x}, x, \hat{u})$ with $i, j \in \{1, 2, \dots, N_R\}$, and use the switching action s_{ij} to select one of them based on the state pair (\hat{x}, q) and the current layer i . More specifically, the probability measures \mathbb{P}_w and $\mathbb{P}_{\hat{w}}$ of their disturbances w and \hat{w} are coupled as follows.

DEFINITION 4.1 (Coupling probability measures). *A coupling [16] of probability measures \mathbb{P}_w and $\mathbb{P}_{\hat{w}}$ on the same measurable space $(\mathbb{W}, \mathcal{B}(\mathbb{W}))$ is any probability measure \mathcal{W}_{ij} on the product measurable space $(\mathbb{W} \times \mathbb{W}, \mathcal{B}(\mathbb{W} \times \mathbb{W}))$ whose marginals are \mathbb{P}_w and $\mathbb{P}_{\hat{w}}$, that is,*

$$\begin{aligned} \mathcal{W}_{ij}(\hat{A} \times \mathbb{W}) &= \mathbb{P}_{\hat{w}}(\hat{A}) \text{ for all } \hat{A} \in \mathcal{B}(\mathbb{W}) \\ \mathcal{W}_{ij}(\mathbb{W} \times A) &= \mathbb{P}_w(A) \text{ for all } A \in \mathcal{B}(\mathbb{W}). \end{aligned}$$

More information about this state-dependent coupling and its influence on the simulation relation can be found in [23, 42].

We can also design \mathcal{W}_{ij} as a measurable function of the current state pair and actions, similar to the interface function. This yields a Borel measurable stochastic kernel associating to each (\hat{u}, \hat{x}, x) a probability measure $\bar{\mathcal{W}}_{ij} : \hat{\mathcal{U}} \times \hat{\mathcal{X}} \times \mathbb{X} \rightarrow \mathcal{P}(\mathbb{W}^2)$ that couples probability measures \mathbb{P}_w and $\mathbb{P}_{\hat{w}}$ as in Definition 4.1.

We can now analyze how close the transitions are (see Fig. 3.5b for visualization) and formally define the multi-layered simulation relation as follows.

DEFINITION 4.2 (Multi-layered simulation relation). *Let the models $\mathbf{M}, \hat{\mathbf{M}} \in \mathcal{M}_{\mathbb{Y}}$, and the interface function \mathcal{U}_v (4.1) be given. If there exists measurable relations $\mathcal{R}_i \subseteq \hat{\mathcal{X}} \times \mathbb{X}$ and Borel measurable stochastic kernels $\bar{\mathcal{W}}_{ij}$ that couple \mathbb{P}_w and $\mathbb{P}_{\hat{w}}$ for $i, j \in \{1, 2, \dots, N_R\}$ such that*

1. $\exists i \in \{1, 2, \dots, N_R\} : (\hat{x}_0, x_0) \in \mathcal{R}_i$,
2. $\forall i \in \{1, 2, \dots, N_R\}, \forall (\hat{x}, x) \in \mathcal{R}_i : \mathbf{d}_{\mathbb{Y}}(\hat{y}, y) \leq \epsilon_i$,
3. $\forall i \in \{1, 2, \dots, N_R\}, \forall (\hat{x}, x) \in \mathcal{R}_i, \forall \hat{u} \in \hat{\mathcal{U}} : (\hat{x}^+, x^+) \in \mathcal{R}_j$ holds with probability at least $1 - \delta_{ij}$ with respect to $\bar{\mathcal{W}}_{ij}$.

Then $\hat{\mathbf{M}}$ is stochastically simulated by \mathbf{M} in a multi-layered fashion, denoted as $\hat{\mathbf{M}} \stackrel{\delta}{\preceq}_{\epsilon} \mathbf{M}$, with precision $\epsilon = [\epsilon_i]_i$ and $\delta = [\delta_{ij}]_{ij}$ for $i, j \in \{1, 2, \dots, N_R\}$. \square

REMARK 1. *This simulation relation differs from the original one in [42, Def. 4], since it contains multiple simulation relations \mathcal{R}_i with different output precision and, therefore, allows for variable precision. Note that for $N_R = 1$, this multi-layered simulation relation becomes equivalent to the simulation relation from [42, Def. 4]. The difference between a simulation relation with a fixed precision and a multi-layered simulation relation with a variable precision is illustrated in Fig. 4.2. Here, we assume ellipsoidal simulation relations, however, the method described in this paper is not restricted to relations with this specific shape.*

The implementation of computing the similarity quantification for LTI systems is detailed in Appendix A.

Running example A (dynamics and simulation relation) Here we present the simulation relations of the homogeneous approach (consisting of 2 DB layers) for the package delivery scenario with specification (3.1) and corresponding regions as before. The dynamics of the car are modeled using an LTI stochastic difference equation as in (A.1) (Appendix A) with $A = 0.9I_2, B = 0.5I_2, B_w = \sqrt{0.25}I_2$, and $C = I_2$. We used states

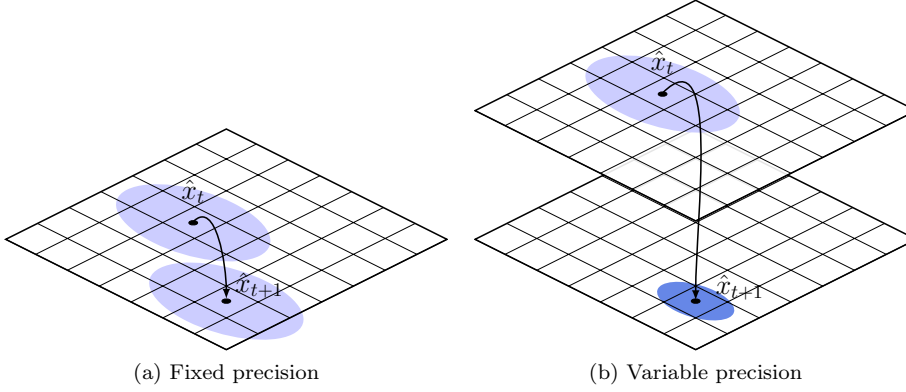


Fig. 4.2: Graphical representation of a probabilistic transition for a fixed precision in (a) and a variable precision with two discretization-based layers in (b). In the left figure, the light blue ellipsoids contain all states x_t resp. x_{t+1} for which it holds that $(\hat{x}_t, x_t) \in \mathcal{R}_1$ resp. $(\hat{x}_{t+1}, x_{t+1}) \in \mathcal{R}_1$. In the right figure, the light blue ellipsoid contains all states x_t for which it holds that $(\hat{x}_t, x_t) \in \mathcal{R}_1$, and the dark blue ellipsoid contains all states x_{t+1} for which it holds that $(\hat{x}_{t+1}, x_{t+1}) \in \mathcal{R}_2$. In both figures, the space discretization or grid size is the same, while the simulation relations \mathcal{R}_1 and \mathcal{R}_2 are ellipsoids with different parameters.

$x \in \mathbb{X} = [-5, 5]^2$, inputs $u \in \mathbb{U} = [-1.25, 1.25]^2$, outputs $y \in \mathbb{Y} = \mathbb{X}$ and Gaussian disturbance $w \sim \mathcal{N}(0, I_2)$. Note that this running example is more challenging than the original running example, as introduced in (3.2) since the input space is reduced.

We construct abstract model $\hat{\mathbf{M}}$ in the form of (A.2) by partitioning the state space with 283×283 regions and the input space with 3×3 regions. We choose interface function $u = \hat{u}$ and simulation relations $\mathcal{R}_i = \{(\hat{x}, x) \in \hat{\mathbb{X}} \times \mathbb{X} \mid \|x - \hat{x}\|_D \leq \epsilon_i\}$, $i \in \{1, 2\}$.

Next, we set the first layer with \mathcal{R}_1 , where $\epsilon_1 = 0.5$ and the second layer with \mathcal{R}_2 , where $\epsilon_2 = 0.3$. Given that we have $\epsilon = [0.5 \quad 0.3]$, we compute δ based on Lemma A.1 in Appendix A. We obtain the weighting matrix $D = I_2$ and deviation bounds as

$$\epsilon = [0.5 \quad 0.3], \quad \delta = \begin{bmatrix} 0 & 0.1586 \\ 0 & 0.0160 \end{bmatrix}.$$

4.2. Homogeneous-layered dynamic programming. After quantifying the similarity, we can synthesize a robust controller and compute a lower bound on the satisfaction probability based on the deviation bounds ϵ and δ . Since we consider specifications written using scLTL, we can formulate this problem as a reachability problem that can be solved as a dynamic programming problem.

scLTL satisfaction as a reachability problem. By converting the scLTL specification ϕ to a DFA \mathcal{A}_ϕ such that the word π satisfies this specification $\pi \models \phi$, iff π is accepted by \mathcal{A}_ϕ , we can reason about the satisfaction of specifications over \mathbf{M} by analyzing its product composition with \mathcal{A}_ϕ [40] denoted as $\mathbf{M} \otimes \mathcal{A}_\phi$. This composition yields a stochastic system with states $(x_t, q_t) \in \mathbb{X} \times Q$ and input u_t . Given input u_t , the stochastic transition from x_t to x_{t+1} of \mathbf{M} is extended to the transition from (x_t, q_t) to (x_{t+1}, q_{t+1}) with $q_{t+1} = \tau_{\mathcal{A}_\phi}(q_t, L(h(x_t)))$. Hence, by computing a Markov

policy over $\mathbf{M} \otimes \mathcal{A}_\phi$ that solves this reachability problem, we obtain a controller with respect to specification ϕ , that has a finite memory [7]. In [42], it is shown that for any gMDP (and other equivalent representations), this reachability problem can be rewritten as a dynamic programming (DP) problem.

Standard robust dynamic programming. The standard robust DP approach detailed in [42] with a single layer is as follows. Given Markov policy $\boldsymbol{\mu} = (\mu_0, \mu_1, \dots, \mu_N)$ with time horizon N for $\mathbf{M} \otimes \mathcal{A}_\phi$, define the time-dependent value function $V_N^\boldsymbol{\mu}$ as

$$(4.2) \quad V_N^\boldsymbol{\mu}(x, q) = \mathbb{E}_\boldsymbol{\mu} \left[\sum_{k=1}^N \mathbf{1}_{Q_f}(q_k) \prod_{j=1}^{k-1} \mathbf{1}_{Q \setminus Q_f}(q_j) \middle| (x_0, q_0) = (x, q) \right]$$

with indicator function $\mathbf{1}_E(q)$ equal to 1 if $q \in E$ and 0 otherwise. Since $V_N^\boldsymbol{\mu}(x, q)$ expresses the probability that a trajectory generated under $\boldsymbol{\mu} : \mathbb{X} \times Q \rightarrow \mathbb{U}$ starting from (x, q) will reach the target set Q_f within the time horizon $[1, \dots, N]$, it also expresses the probability that specification ϕ will be satisfied in this time horizon. Next, define the associated DP operator

$$(4.3) \quad \mathbf{T}^u(V)(x, q) := \mathbb{E}_u(\max\{\mathbf{1}_{Q_f}(q^+), V(x^+, q^+)\}),$$

with $u = \mu(x, q)$, $x^+ := x(t+1)$ evolving according to (2.1), and with the implicit transitions $q^+ = \tau_{\mathcal{A}_\phi}(q, L(h(x^+)))$. Consider a policy $\boldsymbol{\mu}_k = (\mu_{k+1}, \dots, \mu_N)$ with time horizon $N-k$, then it follows that $V_{N-k+1}^{\boldsymbol{\mu}_{k-1}}(x, q) = \mathbf{T}^{\boldsymbol{\mu}_k}(V_{N-k}^{\boldsymbol{\mu}_k})(x, q)$, $\forall (x, q) \in \mathbf{M} \otimes \mathcal{A}_\phi$. Thus if $V_{N-k}^{\boldsymbol{\mu}_k}$ expresses the probability of reaching Q_f within $N-k$ steps, then $\mathbf{T}^{\boldsymbol{\mu}_k}(V_{N-k}^{\boldsymbol{\mu}_k})$ expresses the probability of reaching Q_f within $N-k+1$ steps with policy $\boldsymbol{\mu}_{k-1}$. It follows that for a stationary policy $\boldsymbol{\mu}$, the infinite-horizon value function can be computed as $V_\infty^\boldsymbol{\mu} = \lim_{N \rightarrow \infty} (\mathbf{T}^\boldsymbol{\mu})^N V_0$ with $V_0 \equiv 0$. Furthermore, the optimal DP operator $\mathbf{T}^*(\cdot) := \sup_\boldsymbol{\mu} \mathbf{T}^\boldsymbol{\mu}(\cdot)$ can be used to compute the optimal converged value function V_∞^* . The corresponding satisfaction probability can now be computed as

$$\mathbb{P}^{\boldsymbol{\mu}^*} := \max(\mathbf{1}_{Q_f}(\bar{q}_0), V_\infty^*(x_0, \bar{q}_0)),$$

with $\bar{q}_0 = \tau_{\mathcal{A}_\phi}(q_0, L(h(x_0)))$ and is also denoted as $\mathbb{P}(\mathbf{M} \times \mathbf{C} \models \phi)$. When the policy $\boldsymbol{\mu}^*$, or equivalently the controller \mathbf{C} , yields a satisfaction probability higher than p_ϕ , then (2.3) is satisfied and the synthesis problem is solved.

Due to the continuous states of \mathbf{M} , the DP formulation above cannot be computed for the original model \mathbf{M} , instead, we use abstract model $\hat{\mathbf{M}}$. As a consequence, we have to take deviation bounds ϵ and δ into account. For a fixed precision, this robust DP operator is introduced by [22]. We repeat it here for completeness:

$$(4.4) \quad \mathbf{T}^{\hat{u}}(V)(\hat{x}, q) = \mathbf{L}(\mathbb{E}_{\hat{u}}(\min_{q^+ \in Q_\epsilon^+} \max\{\mathbf{1}_{Q_f}(q^+), V(\hat{x}^+, q^+)\}) - \delta),$$

with $\hat{u} = \mu(\hat{x}, q)$ and $\mathbf{L} : \mathbb{R} \rightarrow [0, 1]$ being a truncation function defined as $\mathbf{L}(\cdot) := \min(1, \max(0, \cdot))$, and with

$$(4.5) \quad Q_\epsilon^+(q, \hat{y}^+) := \{\tau_{\mathcal{A}}(q, L(y^+)) \mid \|y^+ - \hat{y}^+\| \leq \epsilon\}.$$

Note that compared to (4.3), in (4.4) we subtract δ from the expected value to take the deviation in probability into account. Similarly, the deviation in the outputs ϵ can give different labels for the outputs y and \hat{y} . Therefore, we minimize the probability with respect to the possible DFA states associated with these labels. This is done

$$V_N^{\mu_0} \xleftarrow{(4.4)} V_{N-1}^{\mu_1} \leftarrow \dots \leftarrow V_{N-k+1}^{\mu_{k-1}} \xleftarrow{(4.4)} V_{N-k}^{\mu_k} \leftarrow \dots \leftarrow V_1^{\mu_{N-1}} \xleftarrow{(4.4)} V_0^{\mu_N}$$

Fig. 4.3: Graphical representation of the value iteration with a standard robust DP operator. The arguments (\hat{x}, q) , respectively the abstract state and DFA state, of the value functions are omitted for simplicity.

through Q_ϵ^+ as in (4.5). A graphical representation of the value iteration using this robust DP operator is given in Fig. 4.3.

Switching strategy. For the multi-layered approach, we introduce multiple layers. To compute the value function, we need to keep track of the layers. To this end, we use a *switching strategy*. Consider a switching strategy that associates a switching action s_{ij} to state pairs $(\hat{x}, q) \in \hat{\mathbb{X}} \times Q$ depending on the layer i . More specifically, we extend the input action \hat{u} to (\hat{u}, s_{ij}) and split up the corresponding policy as $\boldsymbol{\mu} = (\boldsymbol{\mu}^u, \boldsymbol{\mu}^s)$, with $\boldsymbol{\mu}^u = (\mu_0^u, \mu_1^u, \dots, \mu_N^u)$ and $\boldsymbol{\mu}^s = (\mu_0^s, \mu_1^s, \dots, \mu_N^s)$ determining respectively the input action and switching action, with respectively the mappings $\mu_k^u : \hat{\mathbb{X}} \times Q \times \{1, 2, \dots, N_R\} \rightarrow \hat{\mathbb{U}}$, and $\mu_k^s : \hat{\mathbb{X}} \times Q \times \{1, 2, \dots, N_R\} \rightarrow \mathbb{S}$, $\forall k \in [0, \dots, N]$. Note that for $\boldsymbol{\mu}$, we still have $\boldsymbol{\mu} = (\mu_0, \mu_1, \dots, \mu_N)$, with N the time horizon. For the DP, we are now interested in computing both $\hat{u} = \mu_k^u(\hat{x}, q, i)$ and $s_{ij} = \mu_k^s(\hat{x}, q, i)$ for all $k \in [0, \dots, N]$.

Homogeneous-layered DP. To implement a layered DP approach, we extend the value function to include the different relations \mathcal{R}_i as different layers. Hence, to each layer, we assign a value function $V(\hat{x}, q, i)$. This value function defines a lower bound on the probability that specification ϕ will be satisfied in the time horizon $[1, \dots, N]$. We define a new robust operator $\mathbf{T}_{s_{ij}}^{\hat{u}}$ as

$$\mathbf{T}_{s_{ij}}^{\hat{u}}(V)(\hat{x}, q, i) = \mathbf{L}(\mathbb{E}_{\hat{u}}(\min_{q^+ \in Q_{\epsilon_j}^+} \max \{ \mathbf{1}_{Q_f}(q^+), V(\hat{x}^+, q^+, j) \}) - \delta_{ij}),$$

$$(4.6) \quad \text{with } Q_{\epsilon_j}^+(q, \hat{y}^+) := \{ \tau_{\mathcal{A}}(q, L(y^+)) \mid \|y^+ - \hat{y}^+\| \leq \epsilon_j \}.$$

For given policy $\boldsymbol{\mu} = (\boldsymbol{\mu}^u, \boldsymbol{\mu}^s)$, we define $\mathbf{T}^\mu(V)(\hat{x}, q, i) = \mathbf{T}_{s_{ij}}^{\hat{u}}(V)(\hat{x}, q, i)$ with $\hat{u} = \mu^u(\hat{x}, q, i)$, and $s_{ij} = \mu^s(\hat{x}, q, i)$. Consider a policy $\boldsymbol{\mu}_k = (\mu_{k+1}, \dots, \mu_N)$, then for all (\hat{x}, q, i) we have that $V_{N-k+1}^{\boldsymbol{\mu}_{k-1}} = \mathbf{T}^{\boldsymbol{\mu}_k}(V_{N-k}^{\boldsymbol{\mu}_k})$, initialized with $V_0 \equiv 0$. Fig. 4.4 gives a graphical representation of the multi-layered value iteration for two layers and all possible switching actions. As before, for a stationary policy $\boldsymbol{\mu}$, the infinite-horizon value function for all layers can be computed as $V_\infty^\mu = \lim_{N \rightarrow \infty} (\mathbf{T}^\mu)^N V_0$ with $V_0 \equiv 0$.

REMARK 2. *The DP operator in (4.6) is an adaptation of the operator in (4.4) to a multi-layered setting. For a fixed precision, that is one value for ϵ and one for δ , the DP operators in (4.6) and (4.4) become equivalent, hence we retrieve the DP operator for a fixed precision.*

Following [22], to use the DP operator to compute a lower bound on the satisfaction probability, it should satisfy some properties. The first property is that it is monotonically increasing. Note that a Bellman-operator $\mathbf{T}(\cdot)$ is *monotonically increasing* if for any two functions V and W for which we have that $\forall (\hat{x}, q, i) \in \hat{\mathbb{X}} \times Q \times \{1, 2, \dots, N_R\}$: $V(\hat{x}, q, i) \geq W(\hat{x}, q, i)$, it holds that $\forall j \in \{1, 2, \dots, N_R\}$:

$$\mathbf{T}_{s_{ij}}^{\hat{u}}(V)(\hat{x}, q, i) \geq \mathbf{T}_{s_{ij}}^{\hat{u}}(W)(\hat{x}, q, i).$$

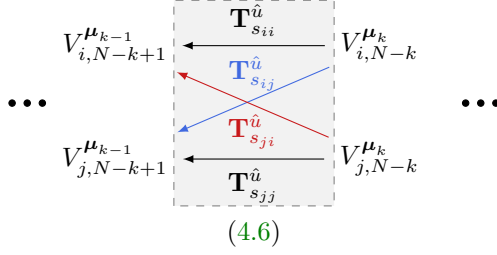


Fig. 4.4: Graphical representation of the value iteration for homogeneous layers, where all possible switching actions $s_{ij} \in \mathbb{S}$ are considered. All operations in the gray box can be performed using (4.6). The arguments (\hat{x}, q, i) and (\hat{x}, q, j) of the value functions in respectively the top and bottom rows are omitted for simplicity. Note that the layer is indicated as a subscript instead. The dots indicate that the full value iteration follows the sequence as in Fig. 4.3.

We can now conclude the following.

THEOREM 4.3. *The robust DP operator in (4.6) is monotonically increasing, and the series $\left\{(\mathbf{T}_{s_{ij}}^{\hat{u}})^k(V_0)\right\}_{k \geq 0}$ with $V_0 \equiv 0$ is monotonically increasing and point-wise converging. Furthermore, the fixed point equation $V_\infty^{\hat{u}} = \mathbf{T}_{s_{ij}}^{\hat{u}}(V_\infty^{\hat{u}})$ has a unique solution for $\delta_{ij} > 0$, which is $V_\infty^{\hat{u}} = \lim_{N \rightarrow \infty} (\mathbf{T}_{s_{ij}}^{\hat{u}})^N V_0$ with $V_0 \equiv 0$.*

Proof. The proof of this theorem follows along the same lines as Lemma 1 in [22], however, in this case, we have an adaptive robust DP operator. The difference is the introduction of the layers and the different values for ϵ_j and δ_{ij} . Since this does not impact the properties in the proof, we can follow the proof of Lemma 1 in [22] to show that the properties in this theorem still hold. \square

The value function gives the probability of satisfying the specification in 1 to ∞ time step, by including the first time instance based on x_0 , we can compute the robust satisfaction probability, that is

$$(4.7) \quad \mathbb{R}^\mu := \max(\mathbf{1}_{Q_f}(\bar{q}_0), \max_{i \in \{1, 2, \dots, N_R\}} V_\infty^\mu(\hat{x}_0, \bar{q}_0, i)),$$

with $\bar{q}_0 = \tau_{\mathcal{A}_\phi}(q_0, L(h(x_0)))$ and $\hat{x}_0 \in \mathcal{R}^{-1}(x_0)$. The robust satisfaction probability as in (4.7) is also denoted as $\mathbb{R}_{\epsilon, \delta}^\mu(\hat{\mathbf{M}} \times \hat{\mathbf{C}} \models \phi)$

To compute the optimal value function V_∞^* , we use the optimal robust operator

$$(4.8) \quad \mathbf{T}^*(\cdot)_{s_{ij}} := \sup_{\mu} \mathbf{T}_{s_{ij}}^\mu(\cdot).$$

The operator $\sup_{\mu}(\cdot)$ implicitly optimizes both over $\hat{u} \in \hat{\mathbb{U}}$ and $j \in \{1, 2, \dots, N_R\}$, which in practice is a very expensive operation with respect to computation time and memory usage. This is especially the case when the number of abstract inputs or the number of layers is large.

4.3. Efficient implementation of homogeneous-layered dynamic programming. In this section, we detail two implementation approaches that improve the computational efficiency.

Optimize the switching strategy using a surrogate model. To reduce the computation time and memory usage, we split the computation of the optimal input policy and switching strategy. To this end, we use the DP operator in (4.6) in two different ways. First to compute a switching strategy, then to compute the abstract input and the robust satisfaction probability. In this section, we detail a practical approach to determine the switching strategy that is close to optimal, while also being efficient with respect to computation time and memory usage.

In (4.8), we determine the optimal action pair (\hat{u}, s_{ij}) , by considering all possible input actions $\hat{u} \in \hat{\mathbb{U}}$ and all possible switching actions $s_{ij} \in \mathbb{S}$ at all states and layers. This computation requires a lot of memory and computation power, therefore we pre-compute an approximately optimal switching strategy. To save computational power, we only compute the switching strategy for an abstract model with an extra coarsely partitioned state space, referred to as the *surrogate model* $\hat{\mathbf{M}}_s$ with state space $\hat{\mathbb{X}}_s$. Note that this surrogate model is a finite-state abstraction of the original model \mathbf{M} that is constructed in the exact same way as finite-state abstraction $\hat{\mathbf{M}}$, however, the grid is a lot coarser for $\hat{\mathbf{M}}_s$ compared to $\hat{\mathbf{M}}$.

The approach to compute the switching strategy using this surrogate model is summarized in Alg. 4.1. After constructing the surrogate model by partitioning the state space with a finite number of grid cells, we compute a suitable switching action using the (ϵ, δ) values corresponding to the actual abstract model $\hat{\mathbf{M}}$. More specifically, we compute the switching action at (\hat{x}, q, i) as

$$(4.9) \quad (\hat{u}^*, s_{ij}^*) = \arg \max_{(\hat{u}, s_{ij})} \mathbf{T}_{s_{ij}}^{\hat{u}}(V)(\hat{x}, q, i),$$

with operator $\mathbf{T}_{s_{ij}}^{\hat{u}}(\cdot)$ as in (4.6), and with $j \in \{1, 2, \dots, N_R\}$. This optimal switching action $s_{ij}^* = \mu_k^s(\hat{x}, q, i)$ is computed at each time step $k \in [0, \dots, N]$, with N the time horizon. Hence, it is used to build up the optimal switching strategy $\boldsymbol{\mu}^s = (\mu_0^s, \mu_1^s, \dots, \mu_N^s)$.

Algorithm 4.1 Optimize switching strategy

- 1: **Input:** $\mathbf{M}, \epsilon, \delta, \mathcal{A}_\phi$
 - 2: $\hat{\mathbf{M}}_s \leftarrow$ Construct surrogate model $\hat{\mathbf{M}}_s$ using a coarse grid.
 - 3: $\boldsymbol{\mu}^s(\hat{x}_s, q, i) \leftarrow$ Perform dynamic programming through (4.6) over all possible switching actions in \mathbb{S} based on model $\hat{\mathbf{M}}_s$ from step 2 and inputs (ϵ, δ) . After convergence is reached, compute optimal switching action using (4.9).
 - 4: $\boldsymbol{\mu}^s(\hat{x}, q, i) \leftarrow$ Translate switching strategy for $\hat{\mathbf{M}}_s$ from step 3 to switching strategy for $\hat{\mathbf{M}}$.
 - 5: **Output:** $\boldsymbol{\mu}^s(\hat{x}, q, i)$
-

Since the DP algorithm determines the best switching action s_{ij} for each abstract state of the surrogate model, it is optimal with respect to this surrogate model. Finally, in step 4, we translate the switching strategy from the surrogate model to the actual abstract model $\hat{\mathbf{M}}$. More specifically, for each $\hat{x} \in \hat{\mathbb{X}}$ we determine the closest (with respect to the L_2 -norm) state $\hat{x}_s \in \hat{\mathbb{X}}_s$ and associate the same switching action s_{ij} to it.

After computing the switching strategy $\boldsymbol{\mu}^s$, the control policy $\boldsymbol{\mu}^u$ is determined for the actual abstract model $\hat{\mathbf{M}}$ together with the robust satisfaction probability. The complete approach is summarized in Alg. 4.2.

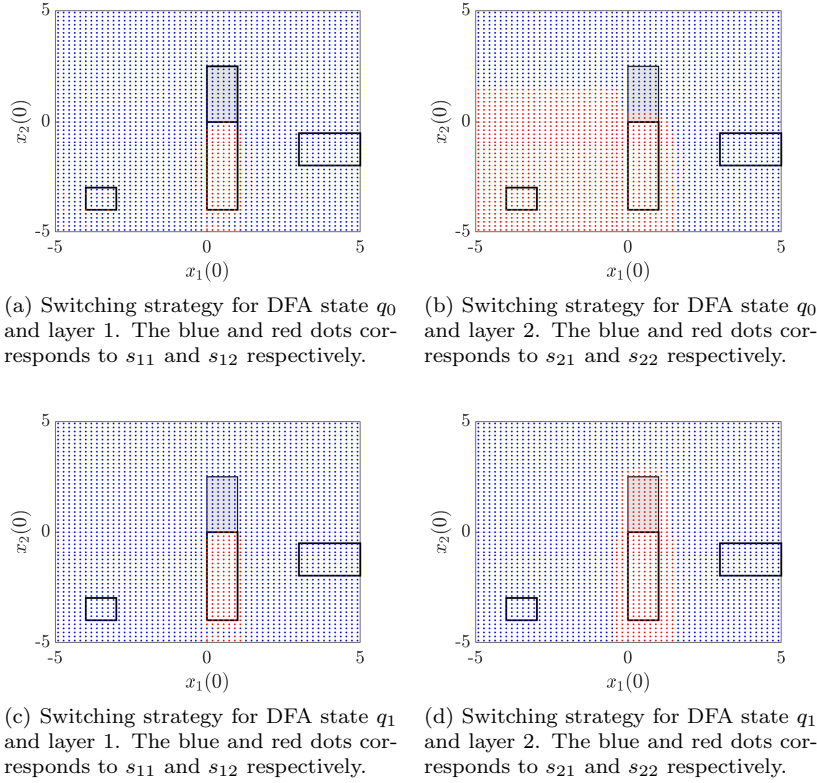


Fig. 4.5: Switching strategy for the states of the surrogate model of running example A for DFA states q_0 in (a), (b) and q_1 in (c), (d). Here, a blue resp. red dot represents switching to layer 1 resp. layer 2. The black boxes indicate regions P_1 , P_2 , P_3 , and P_4 . Region P_2 is colored gray.

Running example A (Switching strategy based on the surrogate model $\hat{\mathbf{M}}_s$). To compute the switching strategy, we construct a surrogate model $\hat{\mathbf{M}}_s$ by partitioning with 55×55 grid cells. This is substantially less than the 283×283 grid cells of the abstract model $\hat{\mathbf{M}}$. By following Alg 4.1, we obtain the optimal switching strategy corresponding to this grid as illustrated in Fig. 4.5. Here, the blue and red dots correspond to switching to layer 1 and layer 2 respectively. From this figure, we can see that this approach is indeed guided by the specification, since depending on the DFA state, the *role* of the P_2 (either *not relevant* or *try to avoid*) is different and the switching strategy changes accordingly.

Partial value iteration. To improve the computational efficiency of our approach even further, we consider layers where we only partially compute the value function. An example is illustrated in Fig. 4.6, where for the gray part of the state space in the high-precision layer, we fix the value function to zero and do not update it. Therefore, the total computation time and memory usage is lower than when performing the value iteration fully. This is especially the case for high-dimensional systems, models with a large number of layers, and models with a large state space.

Algorithm 4.2 Control synthesis

- 1: **Input:** $\mathbf{M}, \hat{\mathbf{M}}, \mathcal{A}_\phi$
 - 2: $(\epsilon, \delta) \leftarrow$ Compute (ϵ, δ) such that $\hat{\mathbf{M}} \preceq_\epsilon^\delta \mathbf{M}$ holds with relation \mathcal{R} .
 - 3: $\mu^s(\hat{x}, q, i) \leftarrow$ Alg. 4.1.
 - 4: $\mu^u(\hat{x}, q, i), \mathbb{R}_{\epsilon, \delta}^\mu(\hat{\mathbf{M}} \times \hat{\mathbf{C}} \models \phi) \leftarrow$ Compute robust controller and satisfaction probability given the switching strategy from step 3.
 - 5: **Output:** $\mu = (\mu^u, \mu^s)$, and $\mathbb{R}_{\epsilon, \delta}^\mu(\hat{\mathbf{M}} \times \hat{\mathbf{C}} \models \phi)$
-

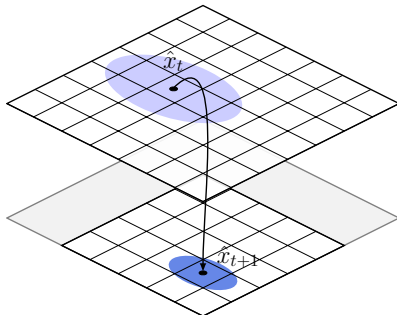


Fig. 4.6: Homogeneous layers with a variable precision, where the value function in the high-precision layer is not fully computed. This part of the high-precision layer (bottom) is given in gray.

4.4. Homogeneous-layered control refinement. The abstract controller $\hat{\mathbf{C}}$ is designed based on the abstract model $\hat{\mathbf{M}}$ in (3.3). Since we take the similarity quantification into account during the control design, we can refine the abstract controller $\hat{\mathbf{C}}$ to a controller \mathbf{C} that can be deployed on the original model \mathbf{M} . In this section, we show that with the given DP approach, such a control refinement is indeed possible and the computed satisfaction probability is valid.

We design the abstract control $\hat{\mathbf{C}}$ based on the abstract model $\hat{\mathbf{M}}$ that is coupled through an interface function \mathcal{U}_v as in (4.1) and a stochastic kernel $\bar{\mathcal{W}}_{ij}$ as in (4.10). Due to this coupling, we can define the combined stochastic difference equation, with finite mode σ_t that keeps track of the layer as

$$(4.10) \quad \hat{\mathbf{M}} \parallel \mathbf{M} : \begin{cases} \begin{pmatrix} \hat{x}_{t+1} \\ x_{t+1} \end{pmatrix} &= \begin{pmatrix} \hat{f}(\hat{x}_t, \hat{u}_t, \hat{w}_t) \\ f(x_t, \mathcal{U}_v(\hat{u}_t, \hat{x}_t, x_t), w_t) \end{pmatrix} \\ \hat{y}_t &= \hat{h}(\hat{x}_t) \\ y_t &= h(x_t) \\ \sigma_{t+1} &= j \text{ if } \sigma_t = i, \text{ and } s_t = s_{ij} \\ (\hat{w}_t, w_t) &\sim \bar{\mathcal{W}}_{ij}(\cdot | \hat{x}, x, \hat{u}) \text{ if } s_t = s_{ij}, \end{cases}$$

with pair of states $(\hat{x}, x) \in \hat{\mathbb{X}} \times \mathbb{X}$, control input $\hat{u} \in \hat{\mathbb{U}}$, outputs $\hat{y}, y \in \mathbb{Y}$, and coupled disturbance (\hat{w}, w) . The input space of this combined system has been extended; that is, next to control input \hat{u}_t we also have a switching input s_t . More specifically, since the disturbances of the combined transitions (4.10) are generated from the stochastic kernel $\bar{\mathcal{W}}_{ij}$, (4.10) holds, with $(\hat{w}, w) \sim \bar{\mathcal{W}}_{ij}$ if $s_t = s_{ij}$. The combined system is illustrated in the gray box in Fig. 4.7a. Given the coupled stochastic difference equation, we can analyze how close the transitions are and therefore, quantify the

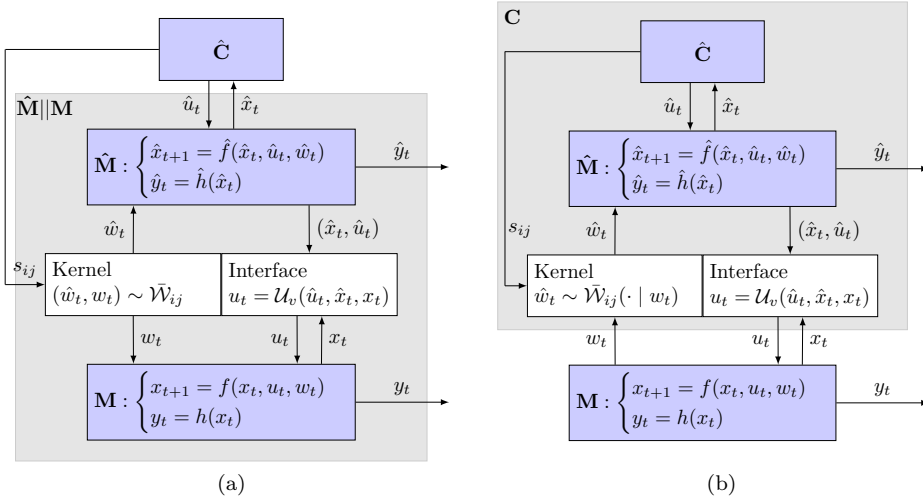


Fig. 4.7: In (a), designing an abstract controller $\hat{\mathbf{C}}$ for coupled transitions of $\hat{\mathbf{M}}||\mathbf{M}$, where the switching action s_{ij} determines the stochastic kernel $\hat{\mathcal{W}}_{ij}$. In (b), refined controller \mathbf{C} deployed on the model \mathbf{M} with conditional kernel $\hat{\mathcal{W}}_{ij}$.

similarity between models (2.1) and (3.3). Furthermore, the additional switching action allows us to do this in a multi-layered manner, as defined in Definition 4.2.

Consider a control strategy μ for $\hat{\mathbf{M}}$, indicated by $\hat{\mathbf{C}}$ in Fig. 4.7a. This strategy can also be implemented on the combined model $\hat{\mathbf{M}}||\mathbf{M}$ and we denote the value function of the combined model as $V_c(\hat{x}, x, q, i)$. The control strategy for the combined model can be refined to a control strategy of the original model \mathbf{M} (2.1), as depicted in Fig. 4.7b. Although $V_c(\hat{x}, x, q, i)$ expresses the probability of satisfaction, it cannot be computed directly, instead we can compute $V(\hat{x}, q, i)$ over the abstract model $\hat{\mathbf{M}}$ using (4.6).

To prove that for any control strategy μ (or controller $\hat{\mathbf{C}}$) for $\hat{\mathbf{M}}||\mathbf{M}$ there still trivially exists a controller \mathbf{C} for \mathbf{M} that preserves the lower bound on the satisfaction probability, it is sufficient to formulate the following lemma.

LEMMA 4.4. *Suppose $\hat{\mathbf{M}} \preceq_{\epsilon}^{\delta} \mathbf{M}$ with a multi-layered simulation relation \mathcal{R} is given. Let $V(\hat{x}, q, j) \leq V_c(\hat{x}, x, q, j)$ for all $(\hat{x}, x) \in \mathcal{R}_j$, then*

$$(4.11) \quad \mathbf{T}_{s_{ij}}^{\hat{u}}(V)(\hat{x}, q, i) \leq \mathbf{T}_{s_{ij}}^{\hat{u}}(V_c)(\hat{x}, x, q, i) \quad \forall (\hat{x}, x) \in \mathcal{R}_i,$$

where $\mathbf{T}_{s_{ij}}^{\hat{u}}(V)(\hat{x}, q, i)$ is the (ϵ, δ) -robust operator (4.6) with respect to stochastic transitions of $\hat{\mathbf{M}}$ and $\mathbf{T}_{s_{ij}}^{\hat{u}}(V_c)(\hat{x}, x, q, i)$ is the exact recursion (4.3) extended to the combined stochastic transitions (4.10).

The proof of Lemma 4.4 follows along the same lines as the proof of Lemma 3 in the extended version of [22]. It is given here for completeness.

Proof. The expected-value part of the operator $\mathbf{T}_{s_{ij}}^{\hat{u}}(V)(\hat{x}, q, i)$ in (4.6) equals

$$(4.12) \quad \mathbb{E}_{\hat{u}} \left(\min_{q^+ \in Q_{\epsilon_j}^+} \max \{ \mathbf{1}_{Q_f}(q^+), V(\hat{x}^+, q^+, j) \} \right) - \delta_{ij}.$$

This expected value can be rewritten to an integral and multiplication with the transition kernel. Hence, (4.12) is equivalent to

$$(4.13) \quad \int_{\hat{\mathbb{X}}} \min_{q^+ \in Q_{\epsilon_j}} \max \{ \mathbf{1}_{Q_f}(q^+), V(\hat{x}^+, q^+, j) \} \mathbf{t}(d\hat{x}^+ | \hat{x}, \hat{u}) - \delta_{ij}.$$

Denote the transition kernel of the combined model $\hat{\mathbf{M}}||\mathbf{M}$ as $\bar{\mathcal{W}}_{ij}^x(\cdot | \hat{x}, x, \hat{u}) : \mathcal{B}(\hat{\mathbb{X}} \times \mathbb{X}) \rightarrow [0, 1]$, which is equivalent to the evolution of the state pair of $\hat{\mathbf{M}}||\mathbf{M}$ as in (4.10), that is

$$\begin{pmatrix} \hat{x}_{t+1} \\ x_{t+1} \end{pmatrix} = \begin{pmatrix} \hat{f}(\hat{x}_t, \hat{u}_t, \hat{w}_t) \\ f(x_t, \mathcal{U}_v(\hat{u}_t, \hat{x}_t, x_t), w_t) \end{pmatrix}$$

with $(\hat{w}_t, w_t) \sim \bar{\mathcal{W}}_{ij}(\cdot | \hat{x}, x, \hat{u}) : \mathcal{B}(\mathbb{W} \times \mathbb{W}) \rightarrow [0, 1]$, written as a transition kernel. For $(\hat{x}, x) \in \mathcal{R}_i$ and input \hat{u} applied to the combined model $\hat{\mathbf{M}}||\mathbf{M}$, the integral in (4.13) is equivalent to the integral

$$\int_{\hat{\mathbb{X}} \times \mathbb{X}} \min_{q^+ \in Q_{\epsilon_j}} \max \{ \mathbf{1}_{Q_f}(q^+), V(\hat{x}^+, q^+, j) \} \bar{\mathcal{W}}_{ij}^x(d\zeta|z) - \delta_{ij},$$

with abbreviation $\bar{\mathcal{W}}_{ij}^x(d\zeta|z) := \bar{\mathcal{W}}_{ij}^x(d\hat{x}^+ \times dx^+ | (\hat{x}, x, \hat{u}))$. For $(\hat{x}, x) \in \mathcal{R}_i$, we can split this integral up using the simulation relation $\mathcal{R}_i \subseteq \hat{\mathbb{X}} \times \mathbb{X}$ and find the following upper bound

$$\begin{aligned} & \int_{\mathcal{R}_i} \min_{q^+ \in Q_{\epsilon_j}} \max \{ \mathbf{1}_{Q_f}(q^+), V(\hat{x}^+, q^+, j) \} \bar{\mathcal{W}}_{ij}^x(d\zeta|z) \\ & + \int_{\hat{\mathbb{X}} \times \mathbb{X} \setminus \mathcal{R}_i} \min_{q^+ \in Q_{\epsilon_j}} \max \{ \mathbf{1}_{Q_f}(q^+), V(\hat{x}^+, q^+, j) \} \bar{\mathcal{W}}_{ij}^x(d\zeta|z) - \delta_{ij} \\ & \leq \int_{\mathcal{R}_i} \min_{q^+ \in Q_{\epsilon_j}} \max \{ \mathbf{1}_{Q_f}(q^+), V(\hat{x}^+, q^+, j) \} \bar{\mathcal{W}}_{ij}^x(d\zeta|z). \end{aligned}$$

Here, we used that $\bar{\mathcal{W}}_{ij}^x((\hat{\mathbb{X}} \times \mathbb{X}) \setminus \mathcal{R}_i | \hat{x}, x, \hat{u}) \leq \delta_{ij}$.

Following the assumption of the lemma, we have that for all $(\hat{x}^+, x^+) \in \mathcal{R}_j$, it holds that $V(\hat{x}^+, q^+, j) \leq V_c(\hat{x}^+, x^+, q^+, j)$. Furthermore, for all $(\hat{x}^+, x^+) \in \mathcal{R}_j$, we have $q^+ = \tau_{\mathcal{A}}(q, L(y^+)) \in Q_{\epsilon_j}^+$. Hence, we can rewrite the last integral over \mathcal{R}_i and find the upper bound

$$\begin{aligned} & \int_{\mathcal{R}_i} \max \{ \mathbf{1}_{Q_f}(q^+), V_c(\hat{x}^+, x^+, q^+, j) \} \bar{\mathcal{W}}_{ij}^x(d\zeta|z) \\ & \leq \int_{\hat{\mathbb{X}} \times \mathbb{X}} \max \{ \mathbf{1}_{Q_f}(q^+), V_c(\hat{x}^+, x^+, q^+, j) \} \bar{\mathcal{W}}_{ij}^x(d\zeta|z), \end{aligned}$$

where the last integral is equal to $\mathbf{T}_{s_{ij}}^{\hat{u}}(V_c)(\hat{x}, x, q, i)$.

By taking the truncation \mathbf{L} to the $[0, 1]$ interval over (4.12), we obtain operator $\mathbf{T}_{s_{ij}}^{\hat{u}}(V)(\hat{x}, q, i)$ as in (4.6). This truncation operation does not alter the steps in the proof, and since $\mathbf{T}_{s_{ij}}^{\hat{u}}(V_c)(\hat{x}, x, q, i)$ naturally falls within the interval $[0, 1]$, Lemma 4.4 is proven. \square

As the combined model represents the extension of $\hat{\mathbf{C}}$ to \mathbf{C} , as depicted in Fig. 4.7b, we can guarantee that the robust satisfaction probability computed using (4.7), gives a lower bound on the actual satisfaction probability of $\mathbf{M} \times \mathbf{C}$. To recap, we quantify their similarity between models \mathbf{M} in (2.1) and $\hat{\mathbf{M}}$ in (3.3) through a multi-layered simulation relation as in Definition 4.2. We use the abstract model $\hat{\mathbf{M}}$ to compute 1) a policy μ or equivalently an abstract controller $\hat{\mathbf{C}} : (\hat{u}, s_{ij}) = \mu(\hat{x}, q, i)$, and 2) the robust satisfaction $\mathbb{R}_{\epsilon, \delta}(\hat{\mathbf{M}} \times \hat{\mathbf{C}} \models \phi)$ as in (4.7). In this computation, we take the deviation bounds (ϵ, δ) , such that we have $\hat{\mathbf{M}} \preceq_{\epsilon}^{\delta} \mathbf{M}$, into account. Based on Lemma 4.4, we can now conclude that this robust satisfaction probability gives a lower bound on the actual satisfaction probability.

THEOREM 4.5. *Given models \mathbf{M} in (2.1), $\hat{\mathbf{M}}$ in (3.3), DFA \mathcal{A}_{ϕ} , and stationary Markov policy μ . If $\hat{\mathbf{M}} \preceq_{\epsilon}^{\delta} \mathbf{M}$ holds, then there exists \mathbf{C} , such that $\mathbb{P}(\mathbf{M} \times \mathbf{C} \models \phi) \geq \mathbb{R}_{\epsilon, \delta}^{\mu}(\hat{\mathbf{M}} \times \hat{\mathbf{C}} \models \phi)$.*

Proof. See proof of Theorem 4 in [22], but now with operator $\mathbf{T}_{s_{ij}}^{\hat{u}}$. Since this robust DP operator has the same properties as the DP operator in [22], the proof follows along the same lines. \square

5. Heterogeneous layers. In this section, we first introduce the switching condition between heterogeneous layers, which lays the foundation for integrating the DF method with the DB method. Then we review the standard dynamic programming technique for one DF layer, based on which we describe the adjusted heterogeneous layered dynamic programming.

5.1. Switching between heterogeneous layers. In this subsection, we are interested in switching between DF layers and DB layers. Denote the switching actions from a DF layer to a DB layer and vice versa as respectively s_{fb} and s_{bf} . For ease of notation, we explain everything for only one DF layer and one DB layer, and we remark on how to deal with multiple DF and DB layers.

In the previous section on the multi-layered approach, we use the inherent contraction of the state dynamics to switch to a layer with higher precision. For heterogeneous layers, this is not possible, since the states of the original model that are associated with the DF layer might not cover the complete state space. More specifically, for the DB layers, all states $x \in \mathbb{X}$ can be mapped to a representative state $\hat{x} \in \hat{\mathbb{X}}$ through the operator $\Pi : \mathbb{X} \rightarrow \hat{\mathbb{X}}$. This does not necessarily hold for the DF layer, due to the sparsity of the sample states x_w . Hence, we have to define when a switch between heterogeneous layers is allowed.

A switch from the DB layer to the DF layer is always from one state $\hat{x} \in \hat{\mathbb{X}}$ to one state $x_w \in \mathbb{X}_w$, but a switch from the DF layer to the DB layer is from one state x_w to a set of states in $\hat{\mathbb{X}}$, denoted as $\hat{A}(x_w) \subseteq \hat{\mathbb{X}}$. We define the conditions of switching between the DF layer and the DB layer as follows.

DEFINITION 5.1 (Conditions for switching). *Given models \mathbf{M} , \mathbf{M}_w (3.6) and $\hat{\mathbf{M}}$, ellipsoidal sets \mathcal{E} , and simulation relation $\mathcal{R} \subset \hat{\mathbb{X}} \times \mathbb{X}$, such that we have $\hat{\mathbf{M}} \preceq_{\epsilon}^{\delta} \mathbf{M}$.*

1. *A switch s_{bf} from state \hat{x} to state x_w is possible, if $\forall x \in \mathcal{R}(\hat{x}) : (x_w, x) \in \mathcal{E}$ holds.*
2. *A switch s_{fb} from state x_w to subset $\hat{A}(x_w)$ is possible, if $\forall x \in \mathcal{E}(x_w), \exists \hat{x} \in \hat{A}(x_w) : (\hat{x}, x) \in \mathcal{R}$ holds.*

REMARK 3. *When there are multiple DB layers with different precision, the conditions in Definition 5.1 are determined for each DB layer.*

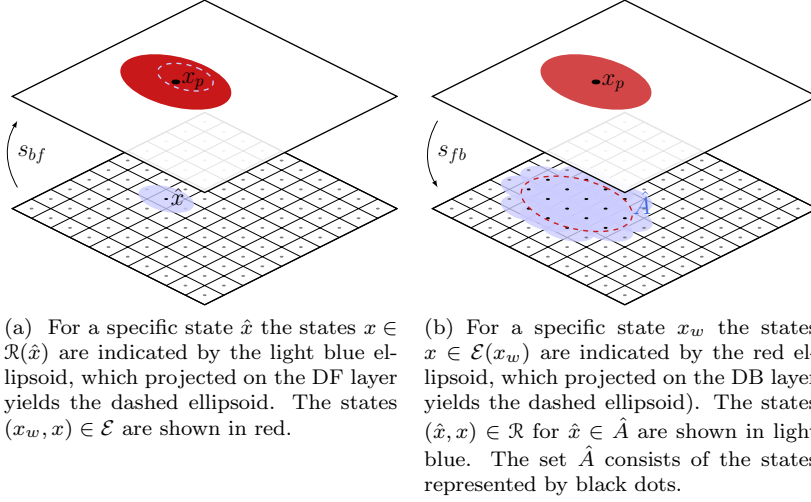


Fig. 5.1: Following respectively conditions 1 and 2 of Definition 5.1, a possibility of switching action s_{bf} from state \hat{x} towards the state x_w is shown in (a). A possibility of switching action s_{fb} from state x_w towards a subset $\hat{A}(x_w)$ is shown in (b).

The conditions of Definition 5.1 can equivalently be written as 1. $\mathcal{R}(\hat{x}) \subseteq \mathcal{E}(x_w)$ and 2. $\mathcal{E}(x_w) \subseteq \mathcal{R}(\hat{A}(x_w))$. In Fig. 5.1 we illustrate these conditions for a specific state and subset $\hat{A}(x_w)$.

5.2. Heterogeneous layered dynamic programming. Let us first introduce the robust DP approach for a single sampling-based layer.

Sampling-based dynamic programming. Denote the value function of the DF layer as $V_{x_w} : \mathbb{X}_w \times Q \rightarrow [0, 1]$. Consider time horizon $[1, \dots, N]$ and a policy $\mu_k = (\mu_{k+1}, \dots, \mu_N)$ with time horizon $N - k$, and with $\mu_k : \mathbb{X}_w \rightarrow \mathbb{X}_w$ that chooses a waypoint x'_w that is reachable from waypoint x_w . We compute the value function at the next iteration as $V_{x_w}^{\text{next}} = V_{x_w, N-k+1}^{\mu_{k-1}} = \mathbf{T}_{x_w}^{\mu_k}(V_{x_w, N-k}^{\mu_k})$, with the Bellman operator defined as

$$\mathbf{T}_{x_w}^{x'_w}(V_{x_w})(x_w, q) = \mathbf{L}(\max\{\mathbf{1}_{Q_f}(q'), V_{x_w}(x'_w, q')\} - (1 - \Delta_w(x_w, x'_w))),$$

with q' the DFA state after n_s time steps, that is $q' = q(t + n_s)$, and with $\Delta_w(x_w, x'_w)$ the probability of reaching x'_w from x_w . Comparing this operator for a sampling-based layer to the one for a discretization-based layer as in (4.4), we can see that in this case, the Bellman operator does not contain an expected value operator anymore. Hence, the value function is computed in a deterministic fashion.

Heterogeneous layered dynamic programming. To distinguish between the value function of the different layers, we denote the value function of the DF layer and DB layer respectively as $V_{x_w} : \mathbb{X}_w \times Q \rightarrow [0, 1]$ and $V_{\hat{x}} : \hat{\mathbb{X}} \times Q \rightarrow [0, 1]$. Consider time horizon $[1, \dots, N]$, then we initially update the value functions of both layers *separately*. To this end, define the updated value functions as $V_{x_w}^{\text{next}} := \mathbf{T}_{x_w}^{\mu_k}(V_{x_w, N-k}^{\mu_k})$ and $V_{\hat{x}}^{\text{next}} := \mathbf{T}_{\hat{x}}^{\mu_k}(V_{\hat{x}, N-k}^{\mu_k})$ with the operators defined in respectively (5.2) and (4.4). After computing the next iteration of the value function for both the DF layer and DB layers, we optimize the switching strategy for each layer. More specifically, we

take the maximum of either staying in the same layer or switching to the other layer to implicitly determine the switching strategy. Furthermore, we take the conditions as defined in Definition 5.1 into account.

For the DF layer, we compute the value function based on $V_{x_w}^{\text{next}}$ and $V_{\hat{x}}^{\text{next}}$. Since, it is not known towards which specific state $\hat{x} \in \hat{A}(x_w)$ we switch, to preserve a lower bound on the satisfaction probability, we consider the worst-case possibility. The value function that takes a possible switch into account can now be given as

$$(5.1) \quad V_{x_w, N-k+1}^{\mu^{k-1}}(x_w, q) = \max \left\{ V_{x_w}^{\text{next}}(x_w, q), \min_{\hat{x} \in \hat{A}(x_w)} \{V_{\hat{x}}^{\text{next}}(\hat{x}, q)\} \right\},$$

with $\hat{A}(x_w) \subset \hat{\mathbb{X}}$ being the set as defined in point 2 of Definition 5.1 if a switch is possible and the empty set, denoted as \emptyset otherwise. If a switch is not possible, hence $\hat{A}(x_w) = \emptyset$, then $\min_{\hat{x} \in \hat{A}(x_w)} \{V_{\hat{x}}^{\text{next}}(\hat{x}, q)\}$ equals zero.

REMARK 4. *When it is allowed to switch from the DF layer towards multiple DB layers according to Definition 5.1, an additional max-operator is required to determine the optimal DB layer to switch towards.*

For the DB layer, we compute the value function as

$$(5.2) \quad V_{\hat{x}, N-k+1}^{\mu^{k-1}}(\hat{x}, q) = \max\{V_{\hat{x}}^{\text{next}}(\hat{x}, q), V_{x_w}^{\text{next}}(\mathcal{S}_{bf}(\hat{x}), q)\}.$$

Here, $\mathcal{S}_{bf} : \hat{\mathbb{X}} \rightarrow \mathbb{X}_w \cup x_\emptyset$, with x_\emptyset an auxiliary state, for which we get $V_{x_w}^{\text{next}}(x_w, q) = V_{x_w}^{\text{next}}(x_\emptyset, q) \equiv 0$, is a function defined as follows

$$\mathcal{S}_{bf}(\hat{x}) = \begin{cases} x_w & \text{if } s_{bf} \text{ is possible from } \hat{x} \text{ to } x_w \text{ (see Def. 5.1),} \\ x_\emptyset & \text{otherwise.} \end{cases}$$

It is trivial to prove that the operations in (5.1) and (5.2) are *monotonically increasing* and *upper bounded by one*. First of all, we can see that (5.1) and (5.2) consist of max- and min-operators and the operators defined in (5.2) and (4.4). Since (5.2) is a minor adaptation of the standard DP operator in (4.4), we can follow Proposition 4.3 to conclude that it is monotonically increasing. Next, we can follow the proof of Lemma 1 in [22] and show that all of the operators that build up these operations preserve an inequality, such as $V(x, q) \geq W(x, q)$.

The overall value function, that is the value function of the total model with multiple heterogeneous layers is denoted as $\bar{V} : (\mathbb{X}_w \sqcup \hat{\mathbb{X}}) \times Q \rightarrow [0, 1]$, with \sqcup the disjoint union. This operator differs from the normal union operator \cup , by keeping the original set membership as a distinguishing characteristic of the union set. Given policy $\bar{\mu}_k = (\bar{\mu}_{k+1}, \dots, \bar{\mu}_N)$, with $\bar{\mu} : (\mathbb{X}_w \sqcup \hat{\mathbb{X}}) \times Q \rightarrow \mathbb{X}_w \times \hat{\mathbb{U}}$, the overall value function is computed iteratively as $\bar{V}_{N-k+1}^{\bar{\mu}^{k-1}} = \bar{\mathbf{T}}^{\bar{\mu}_k}(\bar{V}_{N-k}^{\bar{\mu}_k})$. Here, the overall Bellman-operator $\bar{\mathbf{T}}^{\bar{\mu}_k}(\bar{V}_{N-k}^{\bar{\mu}_k})$ is defined as

$$(5.3) \quad \bar{\mathbf{T}}^{\bar{\mu}_k}(\bar{V}_{N-k}^{\bar{\mu}_k}) = \begin{cases} (5.1) & \text{for } x_w \in \mathbb{X}_w \\ (5.2) & \text{for } \hat{x} \in \hat{\mathbb{X}}. \end{cases}$$

The complete procedure of the value iteration is illustrated in Fig. 5.2.

REMARK 5. *When there are multiple DB layers with different precision, Fig. 5.2 becomes more evolved, and among other changes, equation (4.6) is used instead of (4.4) to take into account switching between the DB layers.*

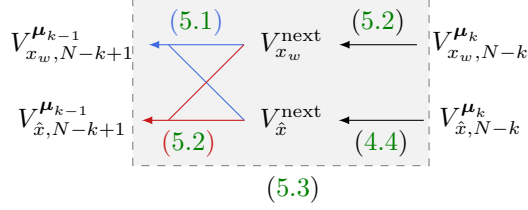


Fig. 5.2: Graphical representation of the value iteration for heterogeneous layers. The operator in (5.3) is equivalent to the complete operation in the gray box. The arguments (x_w, q) and (\hat{x}, q) of the value functions in respectively the top and bottom rows are omitted for simplicity.

We can now conclude the following about the overall Bellman-operator in (5.3).

THEOREM 5.2. *Given any policy $\bar{\mu}$. Suppose that the operations in (5.1) and (5.2) are monotonically increasing and upper bounded by one, then also the overall Bellman-operator $\bar{\mathbf{T}}^{\bar{\mu}^k}(\bar{V}_{N-k}^{\bar{\mu}^k})$ as in (5.3) is monotonically increasing and upper bounded by one.*

Proof. The overall Bellman-operator $\bar{\mathbf{T}}^{\bar{\mu}^k}(\bar{V}_{N-k}^{\bar{\mu}^k})$ as in (5.3) is either computed as (5.1) or (5.2) depending on the considered state. Since both operations in (5.1), and (5.2) are monotonically increasing and upper bounded by one, this also holds for the overall Bellman-operator $\bar{\mathbf{T}}^{\bar{\mu}^k}(\bar{V}_{N-k}^{\bar{\mu}^k})$. \square

As before, the value function gives the probability of satisfying the specification in 1 to ∞ time step, by including the first time instance based on x_0 , we can compute the robust satisfaction probability, that is

$$(5.4) \quad \bar{\mathbb{R}}^{\bar{\mu}} := \max(\mathbf{1}_{Q_f}(\bar{q}_0), \bar{V}_{\infty}^{\bar{\mu}}((x_{w,0}, \hat{x}_0), \bar{q}_0)),$$

with $\bar{q}_0 = \tau_{\mathcal{A}_\phi}(q_0, L(h(x_0)))$, and with $x_{w,0} \in \mathcal{E}^{-1}(x_0)$ and $\hat{x}_0 \in \mathcal{R}^{-1}(x_0)$.

Following the same reasoning as in Section 4.4, we can now conclude that the robust satisfaction probability in (5.4) computed through the overall Bellman-operator $\bar{\mathbf{T}}^{\bar{\mu}^k}(\bar{V}_{N-k}^{\bar{\mu}^k})$ in (5.3) provides a lower bound on the actual satisfaction probability $\mathbb{P}(\mathbf{M} \times \mathbf{C} \models \phi)$.

6. Results. To show the benefits of the multi-layered approach, we consider several case studies. We start with homogeneous layers, where we consider two case studies with increasing complexity. Next, we show that the multi-layered approach with heterogeneous layers outperforms similar single-layered approaches by applying it to a complex case study. All simulations are performed on a computer with a 3.4 GHz 13th Gen Intel Core i7-13700K processor and 64 GB 3200 MHz memory, and use the toolbox SySCoRe [43] as a basis. For each case study, we mention the computation time and memory usage. The computation time is averaged over 5 computations, where we observed a maximum 9% standard deviation. The memory usage is computed as the size of the matrices stored in the workspace.

6.1. Simple reach-avoid specification. Consider a simple reach-avoid specification to park a car in a two-dimensional (2D) space. The goal of the controller is to guarantee that the car parks in area P_1 , without going through area P_2 . This

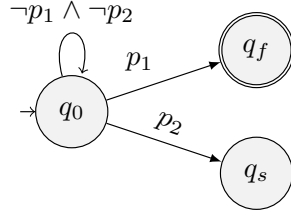


Fig. 6.1: DFA $\mathcal{A}_{\phi_{park}}$ associated with specification $\phi_{park} = \neg p_2 \cup p_1$. The initial, final, and sink state are denoted by respectively q_0, q_f , and q_s .

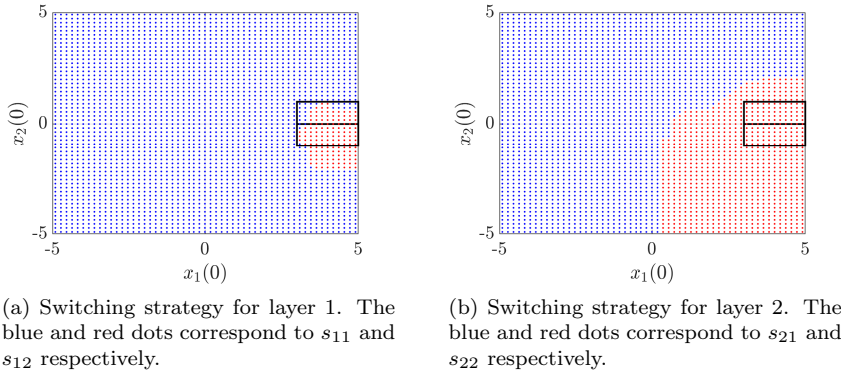


Fig. 6.2: Switching strategy for the states of the surrogate model of the 2D car park case study. Here, a blue resp. red dot represents switching to layer 1 resp. layer 2. The black boxes indicate regions P_1 (bottom) and P_2 (top).

specification can be written as

$$(6.1) \quad \phi_{park} = \neg p_2 \cup p_1,$$

where the labels p_1 , and p_2 correspond to respectively regions P_1 and P_2 , and can be represented by the DFA in Fig. 6.1.

The dynamics of the car are modeled using an LTI stochastic difference equation as in (A.1) with $A = 0.9I_2, B = 0.5I_2$ and $B_w = C = 1$. We used states $x \in \mathbb{X} = [-5, 5]^2$, inputs $u \in \mathbb{U} = [-1, 1]^2$, outputs $y \in \mathbb{Y} = \mathbb{X}$ and Gaussian disturbance $w \sim \mathcal{N}(0, 0.5)$. Furthermore, we have regions $P_1 = [3, 5] \times [-1, 0]$ and $P_2 = [3, 5] \times [0, 1]$ defined on the output space \mathbb{Y} and labeled as respectively p_1 and p_2 .

We computed deviation bounds (ϵ, δ) that satisfy Lemma A.1 as

$$\epsilon = [0.5 \quad 0.2], \quad \delta = \begin{bmatrix} 0 & 0.168 \\ 0 & 0.0169 \end{bmatrix}.$$

Next, we obtained a surrogate model by partitioning with 55×55 grid cells and found the optimal switching strategy¹ corresponding to this grid as illustrated in Fig. 6.2.

Then, we constructed abstract model $\bar{\mathbf{M}}$ in the form of (A.2) by partitioning with 283×283 regions leading to $\mathcal{B} = [-0.0353, 0.0353]^2$. We quantified the accuracy

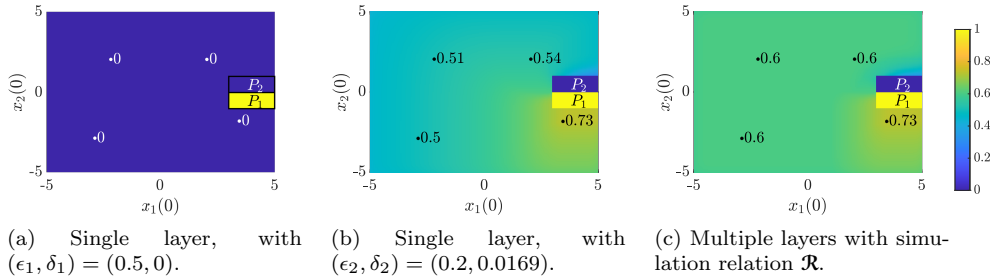


Fig. 6.3: Robust satisfaction probability of the 2D car park case study where a single layer is used in (a) and (b). A multi-layered simulation relation, with switching strategy as in Fig. 6.2 is used in (c).

of $\hat{\mathbf{M}}$ with a bi-layered simulation relation \mathcal{R} and obtained the robust satisfaction probability in Fig. 6.3c. The average computation time is 34.4 seconds while using a memory of 243 MB. The robust satisfaction probability of the multi-layered approach is higher everywhere compared to only using a single layer, with either \mathcal{R}_1 , with $(\epsilon_1, \delta_1) = (0.5, 0)$ or \mathcal{R}_2 , with $(\epsilon_2, \delta_2) = (0.2, 0.0169)$ as can be seen in Fig. 6.3.

6.2. Package delivery specification. Next, we revisit running example A by repeating the important steps. We also show the satisfaction probability and compare it to single-layered approaches. As described throughout the paper, we consider a package delivery scenario with specification (3.1), with its corresponding DFA given in Fig. 3.1. Based on Appendix A and Lemma A.1, we found total deviation bounds

$$\epsilon = [0.5 \quad 0.3], \quad \delta = \begin{bmatrix} 0 & 0.1586 \\ 0 & 0.0160 \end{bmatrix}.$$

Next, we obtained a surrogate model by partitioning with 55×55 grid cells and found a switching strategy by following Alg. 4.1. The optimal switching strategy corresponding to this grid is illustrated in Fig. 4.5. Then, we constructed abstract model $\hat{\mathbf{M}}$ in the form of (A.2) by partitioning the state space with 283×283 regions and the input space with 3×3 regions. We obtained the robust satisfaction probability for DFA states q_0 and q_1 in respectively Fig. 6.4c and 6.4f. The average computation time is 50 seconds while using a memory of 340 MB. The robust satisfaction probability of the multi-layered approach is higher everywhere compared to only using a single layer, as can be seen in Fig. 6.4.

6.3. Case study with heterogeneous layers. To show the benefit of having heterogeneous layers, we apply it to a case study with the same complex reach-avoid specification as before, whose DFA is given in Fig. 3.1.

The system dynamics are the same as of the running example. In terms of comparison to the system dynamics in Section 6.2, the state space is enlarged to $\mathbb{X} = [-20, 5]^2$, the input space to $\mathbb{U} = [-5, 5]^2$, and output space to $\mathbb{Y} = \mathbb{X}$. The full dynamics are given in (3.2).

For this case study, we implement heterogeneous layers with one DF and one DB layer, while we consider a different amount of waypoints in the DF layer. For the sampling-based layer, we chose $\Delta_w = 0.0001$. To obtain a good accuracy for the heterogeneous approach, Δ_w of the DF layer, should be substantially smaller than

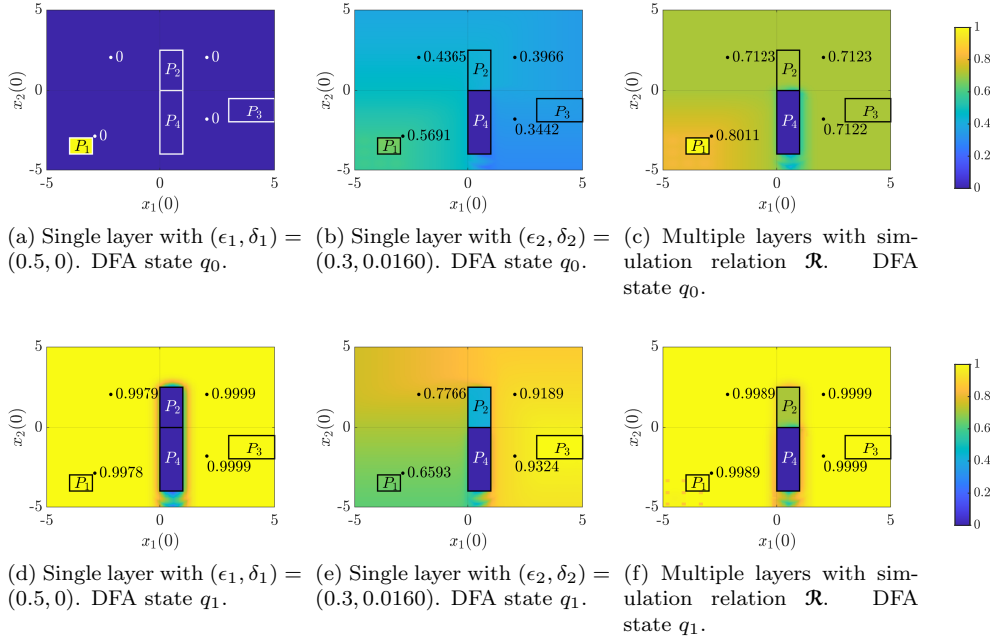


Fig. 6.4: Robust satisfaction probability of package delivery case for DFA state q_0 in (a)-(c) and for DFA state q_1 in (d)-(f). Here, a single layer is used in (a),(b), and (d),(e). A multi-layered simulation relation, with switching strategy as in Fig. 4.5 is used in (c) and (f).

δ of the DB layer. It is in general, a good idea to choose Δ_w very small. We have matrix $D_w = I_2$ for the set \mathcal{E} as in (3.5). To decrease the size of the set \mathcal{E} , we used an interface function (4.1) equal to $u_t = u_{w,t} + K(x_t - x_{w,t})$, with $K = -1.4I_2$. Following the derivation in the appendix, we computed $\epsilon_w = 2.6825$ for set \mathcal{E} in (3.5).

For the discretization-based layer, we compute a finite-state abstraction as in (A.2) by gridding part of the state space $[-9, 5] \times [-5, 3]$ with 318×180 grid cells. We compute the similarity quantification between the original model \mathbf{M} (A.1) and its finite-state abstraction $\hat{\mathbf{M}}$ (A.2) for interface function $u = \hat{u}$, and obtained $(\epsilon, \delta) = (0.18, 0.1217)$.

Next, we perform a value iteration and synthesize a controller using the technique described in Section 5. The robust satisfaction probability obtained with 48 initial waypoints² is shown in Fig. 6.5. The satisfaction probability for the sample states is depicted as ellipsoids. The average computation time equals 5.05 seconds, while using a memory of 653 MB. When increasing the number of waypoints from 48 to 180, the average computation time increases from 5.05 to 9.64 seconds, while the memory usage is the same. The accuracy has not changed substantially, except for a larger coverage of the state space by the sampling-based layer. Hence, we omit the figure with the satisfaction probability.

²The term *initial waypoints* refers to the number of waypoints initially supplied to the algorithm. The number of waypoints in the end may be smaller due to checking well-posedness or larger due to re-sampling.

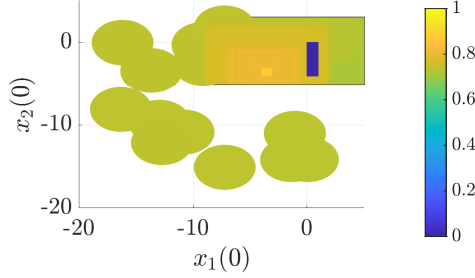


Fig. 6.5: Robust satisfaction probability of package delivery case with enlarged spaces (Section 6.3) when using a multi-layered approach with heterogeneous layers. We used $(\epsilon, \delta) = (0.18, 0.1217)$ for the DB layer with gridded area $[-9, 5] \times [-5, 3]$, and $\epsilon_w = 2.6825, \Delta_w = 0.0001$ for the DF layer.

Table 6.1: Comparison between the multi-layered approach with heterogeneous layers and the corresponding single-layered approaches. The table includes satisfaction probabilities, computation time and memory usage. Here, *DB*, *DF* denote respectively a single-layered *discretization-based* or *discretization-free* approach. *DB+DF* denotes the multi-layered approach with heterogeneous layers. *Sat. prob.* abbreviates *satisfaction probability* and the minimal (nonzero) satisfaction probability is listed here. *Comp. time* abbreviates *Computation time*.

Approach	Figure	Gridded area	Grid size	Grid cells	Sat. prob.	Comp. time (s)	Memory (MB)
<i>DB</i>	3.3a	$[-20, 5]^2$	$[0.0440 \times 0.0444]$	$[568 \times 563]$	0.6846	14.4	2706
<i>DF</i>	3.3b	n.a.	n.a.	n.a.	0	0.3974	0.0268
<i>DB+DF</i>	6.5	$[-9, 5] \times [-5, 3]$	$[0.0440 \times 0.0444]$	$[318 \times 180]$	0.7343	5.05	653

Comparison between a single-layered approach and a multi-layered approach with heterogeneous layers.

Next, we make a fair comparison between the different approaches. First, we consider only a discretization-based approach, where we gridded the complete state space with 568×563 grid cells. Note that the grid size is now almost equal to the one we obtained before. We compute the similarity quantification between the original model \mathbf{M} (A.1) and its finite-state abstraction $\hat{\mathbf{M}}$ (A.2) for interface function $u = \hat{u}$, and obtained $(\epsilon, \delta) = (0.18, 0.1217)$. The robust satisfaction probability is shown in Fig. 3.3a. The computation time equals 14.4 seconds while using a memory of 2706 MB. Next, we consider only a sampling-based approach, where we used $\epsilon_w = 2.6825$ and obtained 48 waypoints. The robust satisfaction probability is shown in Fig. 3.3b. Here, we see that it gives 0 for all robust satisfaction probabilities of waypoints $x_w \in \mathbb{X}_w$, due to the large set \mathcal{E} . The computation time equals 0.3974 seconds while using a memory of 0.0268 MB. It should be noted that due to the large set \mathcal{E} , we cannot obtain a strongly connected graph.

Comparing the satisfaction probabilities in Fig. 6.5 and in Fig. 3.3 we see that the robust satisfaction probability of the heterogeneous-layered approach in Fig. 6.5 is higher than when using either only a discretization-based layer (see Fig. 3.3a) or only a sampling-based layer (see Fig. 3.3b). The results are summarized in Table 6.1. Here, we see that the heterogeneous approach outperforms the discretization-based approach on accuracy (satisfaction probability), computation time, and memory us-

age. Therefore, we conclude that the multi-layered approach with heterogeneous layers outperforms the single-layered approach with either a sampling-based technique or a discretization-based technique.

7. Conclusions. In this paper, we proposed a multi-layered approach that allows us to switch between multiple simulation relations (homogeneous layers) and multiple abstraction-based techniques (heterogeneous layers). This approach makes it possible to use the advantages of each individual layer guided by the given specification, hence providing an efficient and less conservative computational approach for temporal logic control. We illustrated the benefits of the proposed multi-layered approach with homogeneous and heterogeneous layers by applying it to multiple case studies. They all show the improved accuracy of the computations, and the case study with heterogeneous layers indicated a significant increase of 65% in computational efficiency.

In the future, we plan to integrate a comprehensive implementation of the approach within the tool `SySCoRe` [43], which enhances its practical applicability and ease of use. An interesting topic for future research is to develop the theoretical details for allowing multiple discretization-based abstract models with different grid sizes and integrating abstraction-free methods that are based on the concepts of barrier certificates.

REFERENCES

- [1] A. Abate, H. Blom, M. Bouissou, N. Cauchi, H. Chraïbi, J. Delicarîs, S. Haesaert, A. Hartmanns, M. Khaled, A. Lavaei, et al. ARCH-COMP21 category report: Stochastic models. In *8th International Workshop on Applied Verification of Continuous and Hybrid Systems, (ARCH 2021)*, pages 55–89. EasyChair, 2021.
- [2] A. Abate, H. Blom, N. Cauchi, J. Delicarîs, A. Hartmanns, M. Khaled, A. Lavaei, C. Pilch, A. Remke, S. Schupp, et al. ARCH-COMP20 category report: Stochastic models. *EPiC Series in Computing*, 74:pp. 76–106, 2020.
- [3] A. Abate, H. Blom, J. Delicarîs, S. Haesaert, A. Hartmanns, B. C. van Huijgevoort, A. Lavaei, H. Ma, M. Niehage, A. Remke, et al. Arch-comp22 category report: Stochastic models. In *Proceedings of 9th International Workshop on Applied Verification of Continuous and Hybrid Systems, (ARCH 2022)*, volume 90, pages 113–141. EasyChair, 2022.
- [4] A. Abate, M. Prandini, J. Lygeros, and S. Sastry. Probabilistic reachability and safety for controlled discrete time stochastic hybrid systems. *Automatica*, 44(11):pp. 2724–2734, 2008.
- [5] M. Althoff, O. Stursberg, and M. Buss. Computing reachable sets of hybrid systems using a combination of zonotopes and polytopes. *Nonlinear analysis: hybrid systems*, 4(2):233–249, 2010.
- [6] G. R. Belitskii and Y. I. Lyubich. *Matrix norms and their applications*. Birkhäuser Verlag, 1988.
- [7] C. Belta, B. Yordanov, and E. A. Gol. *Formal methods for discrete-time dynamical systems*, volume 15. Springer, 2017.
- [8] S. Bogomolov, M. Forets, G. Frehse, K. Potomkin, and C. Schilling. Juliareach: a toolbox for set-based reachability. In *Proceedings of the 22nd ACM International Conference on Hybrid Systems: Computation and Control*, pages 39–44, 2019.
- [9] J. Cámara, A. Girard, and G. Gössler. Safety controller synthesis for switched systems using multi-scale symbolic models. In *50th IEEE CDC and ECC conference*, pages 520–525. IEEE, 2011.
- [10] J. Cámara, A. Girard, and G. Gössler. Synthesis of switching controllers using approximately bisimilar multiscale abstractions. In *14th HSCC conference*, pages 191–200, 2011.
- [11] N. Cauchi and A. Abate. StocHy-automated verification and synthesis of stochastic processes. *Proc. of the 22nd ACM International Conference on Hybrid Systems: Computation and Control*, pages 258–259, 2019.
- [12] N. Cauchi, L. Laurenti, M. Lahijanian, A. Abate, M. Kwiatkowska, and L. Cardelli. Efficiency through uncertainty: scalable formal synthesis for stochastic hybrid systems. In *HSCC*,

- pages 240–251, 2019.
- [13] V. Chew. Confidence, prediction, and tolerance regions for the multivariate normal distribution. *Journal of the American Statistical Association*, 61(315):605–617, 1966.
 - [14] A. Clark. Control barrier functions for stochastic systems. *Automatica*, 130:109688, 2021.
 - [15] S. R. Cominesi, M. Farina, L. Giulioni, B. Picasso, and R. Scattolini. A two-layer stochastic model predictive control scheme for microgrids. *IEEE Transactions on Control Systems Technology*, 26(1):1–13, 2017.
 - [16] F. den Hollander. *Probability theory: The coupling method (lecture notes)*. Math. Inst. Leiden Univ., The Netherlands, 2012.
 - [17] M. H. W. Engelaar, Z. Zhang, M. Lazar, and S. Haesaert. Risk-aware mpc for stochastic systems with runtime temporal logics. *arXiv preprint arXiv:2402.03165*, 2024.
 - [18] S. S. Farahani, R. Majumdar, V. S. Prabhu, and S. Soudjani. Shrinking horizon model predictive control with chance-constrained signal temporal logic specifications. In *2017 American Control Conference (ACC)*, pages 1740–1746, 2017.
 - [19] A. Girard. Controller synthesis for safety and reachability via approximate bisimulation. *Automatica*, 48(5):947–953, 2012.
 - [20] A. Girard and G. Gössler. Safety synthesis for incrementally stable switched systems using discretization-free multi-resolution abstractions. *Acta Informatica*, 57(1):245–269, 2020.
 - [21] S. Haesaert, R. Babuska, and A. Abate. Sampling-based approximations with quantitative performance for the probabilistic reach-avoid problem over general markov processes. *arXiv preprint arXiv:1409.0553*, 2014.
 - [22] S. Haesaert and S. Soudjani. Robust dynamic programming for temporal logic control of stochastic systems. *IEEE Transactions on Automatic Control*, 66(6):2496–2511, 2020.
 - [23] S. Haesaert, S. Soudjani, and A. Abate. Verification of general Markov decision processes by approximate similarity relations and policy refinement. *SIAM Journal on Control and Optimization*, 55(4):pp. 2333–2367, 2017.
 - [24] K. Hsu, R. Majumdar, K. Mallik, and A. Schmuck. Multi-layered abstraction-based controller synthesis for continuous-time systems. In *21st HSCC conference*, pages 120–129, 2018.
 - [25] P. Jagtap, S. Soudjani, and M. Zamani. Formal synthesis of stochastic systems via control barrier certificates. *IEEE Transactions on Automatic Control*, 66(7):3097–3110, 2020.
 - [26] O. Kupferman and M. Y. Vardi. Model checking of safety properties. *Formal Methods in System Design*, 19(3):pp. 291–314, 2001.
 - [27] A. Lavaei, S. Soudjani, A. Abate, and M. Zamani. Automated verification and synthesis of stochastic hybrid systems: A survey. *Automatica*, 146:110617, 2022.
 - [28] M. Lorenzen, F. Dabbene, R. Tempo, and F. Allgöwer. Constraint-tightening and stability in stochastic model predictive control. *IEEE Transactions on Automatic Control*, 62(7):3165–3177, 2016.
 - [29] F. B. Mathiesen, M. Lahijanian, and L. Laurenti. Intervalmdp. jl: Accelerated value iteration for interval markov decision processes. *arXiv preprint arXiv:2401.04068*, 2024.
 - [30] A. Mesbah. Stochastic model predictive control: An overview and perspectives for future research. *IEEE Control Systems Magazine*, 36(6):30–44, 2016.
 - [31] A. Mesbah. Stochastic model predictive control with active uncertainty learning: A survey on dual control. *Annual Reviews in Control*, 45:107–117, 2018.
 - [32] S. Prajna, A. Jadbabaie, and G. J. Pappas. A framework for worst-case and stochastic safety verification using barrier certificates. *IEEE Transactions on Automatic Control*, 52(8):1415–1428, 2007.
 - [33] W. Ren and D. V. Dimarogonas. Dynamic quantization based symbolic abstractions for nonlinear control systems. In *IEEE 58th CDC conference*, pages 4343–4348. IEEE, 2019.
 - [34] C. Santoyo, M. Dutreix, and S. Coogan. A barrier function approach to finite-time stochastic system verification and control. *Automatica*, 125:109439, 2021.
 - [35] S. Soudjani and A. Abate. Adaptive and sequential gridding procedures for the abstraction and verification of stochastic processes. *SIAM Journal on Applied Dynamical Systems*, 12(2):921–956, 2013.
 - [36] S. Soudjani and A. Abate. Adaptive and sequential gridding procedures for the abstraction and verification of stochastic processes. *SIAM Journal on Applied Dynamical Systems*, 12(2):921–956, 2013.
 - [37] S. Soudjani, C. Gevaerts, and A. Abate. FAUST²: Formal Abstractions of Uncountable-STate STOchastic Processes. *TACAS*, pages 272–286, 2015.
 - [38] P. Tabuada. *Verification and control of hybrid systems: a symbolic approach*. Springer Science & Business Media, 2009.
 - [39] Y. Tazaki and J. Imura. Approximately bisimilar discrete abstractions of nonlinear systems using variable-resolution quantizers. In *2010 ACC conference*, pages 1015–1020, 2010.

- [40] I. Tkachev, A. Mereacre, J. P. Katoen, and A. Abate. Quantitative automata-based controller synthesis for non-autonomous stochastic hybrid systems. In *16th HSCC conference*, pages 293–302, 2013.
- [41] B. C. van Huijgevoort and S. Haesaert. Multi-layered simulation relations for linear stochastic systems. *2021 European Control Conference (ECC)*, pages 728–733, 2021.
- [42] B. C. van Huijgevoort and S. Haesaert. Similarity quantification for linear stochastic systems: A coupling compensator approach. *Automatica*, 144:110476, 2022.
- [43] B. C. van Huijgevoort, O. Schön, S. Soudjani, and S. Haesaert. Syscore: Synthesis via stochastic coupling relations. In *Proceedings of the 26th ACM International Conference on Hybrid Systems: Computation and Control*, pages 1–11, 2023.
- [44] B. C. van Huijgevoort, S. Weiland, and S. Haesaert. Temporal logic control of nonlinear stochastic systems using a piecewise-affine abstraction. *IEEE Control Systems Letters*, 2022.
- [45] C. I. Vasile and C. Belta. Sampling-based temporal logic path planning. In *2013 IEEE/RSJ International Conference on Intelligent Robots and Systems*, pages 4817–4822. IEEE, 2013.
- [46] A. P. Vinod, J. D. Gleason, and M. M. K. Oishi. SReachTools: A MATLAB stochastic reachability toolbox. *Proc. of the 22nd ACM International Conference on Hybrid Systems: Computation and Control*, pages 33–38, 2019.
- [47] B. Wooding and A. Lavaei. Impact: A parallelized software tool for imdp construction and controller synthesis with convergence guarantees. In *Proceedings of the 27th ACM International Conference on Hybrid Systems: Computation and Control*, pages 1–2, 2024.

Appendix A. Implementation of similarity quantification for LTI systems. In this section, we elaborate on how to compute the deviation bounds (ϵ, δ) such that $\hat{\mathbf{M}} \preceq_{\epsilon}^{\delta} \mathbf{M}$ holds (step 2 of Alg. 4.2). The derivation is given for linear time-invariant (LTI) systems but can be extended to nonlinear stochastic systems following the techniques described in [44]. The approach detailed next, follows the same reasoning as in [42], but we made adaptations such that it suits the multi-layered setting.

Let the models \mathbf{M} (2.1) and $\hat{\mathbf{M}}$ (3.3) be linear time-invariant (LTI) systems whose behavior is described by the following stochastic difference equations

$$(A.1) \quad \mathbf{M} : \begin{cases} x(t+1) = Ax(t) + Bu(t) + B_w w(t) \\ y(t) = Cx(t), \text{ and} \end{cases}$$

$$(A.2) \quad \hat{\mathbf{M}} : \begin{cases} \hat{x}(t+1) = \Pi(A\hat{x}(t) + B\hat{u}(t) + B_w \hat{w}(t)) \\ \hat{y}(t) = C\hat{x}(t), \end{cases}$$

with matrices A, B, B_w and C of appropriate sizes and with the disturbances $w(t), \hat{w}(t)$ having the standard Gaussian distribution, i.e., $w(t) \sim \mathcal{N}(0, I) = \mathbb{P}_w$ and $\hat{w}(t) \sim \mathcal{N}(0, I) = \mathbb{P}_{\hat{w}}$. The abstract model is constructed by partitioning the state space \mathbb{X} in a finite number of regions $\mathbb{A}_j \subset \mathbb{X}$ and operator $\Pi(\cdot) : \mathbb{X} \rightarrow \hat{\mathbb{X}}$ maps states $x \in \mathbb{A}_j$ to their representative points³ $\hat{X}_j \in \hat{\mathbb{X}}$. We assume that the regions \mathbb{A}_j are designed in such a way that the set $\mathcal{B} := \bigcup_j \{\hat{X}_j - x_j | x_j \in \mathbb{A}_j\}$ is a bounded polytope and has vertices $\text{vert}(\mathcal{B})$. Details on constructing such an abstract LTI system can be found in [42].

To compute the multi-layered simulation relations in Definition 4.2, we choose the interface function $u(t) = \mathcal{U}_v(\hat{u}_t, \hat{x}_t, x_t) = \hat{u}(t)$ and consider simulation relations \mathcal{R}_i

$$(A.3) \quad \mathcal{R}_i := \left\{ (\hat{x}, x) \in \hat{\mathbb{X}} \times \mathbb{X} \mid \|x - \hat{x}\|_D \leq \epsilon_i \right\},$$

³In general, any point in the region \mathbb{A}_j can be its representative point, but in practice the center has computational benefits.

where $\|x\|_D = \sqrt{x^T D x}$ with D a symmetric positive definite matrix $D = D^T \succ 0$. We use the same weighting matrix D for all simulation relations \mathcal{R}_i , with $i \in \{1, 2, \dots, N_R\}$. The simulation relations in (A.3) have an ellipsoidal shape and for fixed precision such ellipsoids are illustrated in Fig. 4.2a. A switch from one simulation relation to the other one is similarly illustrated in Fig. 4.2b.

For these relations (A.3), condition 1 in Definition 4.2 is satisfied by choosing weighting matrix $D \succ 0$, such that

$$(A.4) \quad C^T C \preceq D.$$

We can now construct kernels $\bar{\mathcal{W}}_{ij}$ using a coupling compensator as introduced in [42]. By doing so, condition 2 of Definition 4.2 can be quantified via contractive sets for the error dynamics $x_{t+1} - \hat{x}_{t+1}$ based on the combined transitions (4.10). We assume that there exist factors $\alpha_{ij} \in [0, 1]$ with $\epsilon_j = \alpha_{ij} \epsilon_i$ that represent the set contraction between the different simulation relations. Now, we can describe the satisfaction of condition 2 as a function of δ_{ij}, α_{ij} and ϵ_i .

LEMMA A.1. *Consider models \mathbf{M} in (A.1) and $\hat{\mathbf{M}}$ in (A.2) for which simulation relations \mathcal{R}_i as in (A.3) are given with weighting matrix D satisfying (A.4). Given δ_{ij}, α_{ij} , and ϵ_i , if there exist parameters λ_{ij} and matrices F_{ij} such that the matrix inequalities*

$$(A.5a) \quad \begin{bmatrix} \frac{1}{\epsilon_i^2} D & F_{ij}^T \\ F_{ij} & r_{ij}^2 I \end{bmatrix} \succeq 0, \quad (\text{input bound})$$

$$(A.5b) \quad \begin{bmatrix} \lambda_{ij} D & * & * \\ 0 & (\alpha_{ij}^2 - \lambda_{ij}) \epsilon_i^2 & * \\ D(A+B_w F_{ij}) & D\beta_l & D \end{bmatrix} \succeq 0 \quad (\text{contraction})$$

are satisfied, then there exists a $\bar{\mathcal{W}}_{ij}$ such that condition 2 in Definition 4.2 is satisfied. The matrix inequalities in (A.5) are parameterized with $\lambda_{ij} > 0$ and should hold for all $\beta_l \in \text{vert}(\mathcal{B})$. Furthermore, r_{ij} is computed as a function of δ_{ij} , that is $r_{ij} = |2 \text{idf}\left(\frac{1-\delta_{ij}}{2}\right)|$, with idf denoting the inverse distribution function of the standard Gaussian distribution. \square

This lemma allows us to conclude the following.

THEOREM A.2. *Consider models \mathbf{M} in (A.1) and $\hat{\mathbf{M}}$ in (A.2) for which simulation relations \mathcal{R}_i as in (A.3) are given with weighting matrix D satisfying (A.4). If the inequalities (A.5) hold for all $i, j \in \{1, \dots, N_R\}^2$ and there exists $i \in \{1, \dots, N_R\}$ such that $(\hat{x}_0, x_0) \in \mathcal{R}_i$ then $\hat{\mathbf{M}}$ is stochastically simulated by \mathbf{M} in a multi-layered fashion as in Definition 4.2, denoted as $\hat{\mathbf{M}} \preceq_\epsilon^\delta \mathbf{M}$.*

Proof. The proof of both Lemma A.1 and Theorem A.2 build on top of the proofs of Theorem 8 and Theorem 9 in [42] for controlled invariant sets. Instead of invariant sets, the proof uses contractive sets to handle the multi-layered simulation relation.

For the construction of the matrix inequalities in (A.5), we follow [42] and model the state dynamics of the abstract model (A.2) as $\hat{x}(t+1) = A\hat{x}(t) + B\hat{u}(t) + B_w(\hat{w}_\gamma(t) - \gamma(t)) + \beta(t)$ with disturbance $\hat{w}_\gamma \in \mathbb{W} \subseteq \mathbb{R}^{n_w}$, shift $\gamma \in \Gamma$ and deviation $\beta \in \mathcal{B}$. The disturbance is generated by a Gaussian distribution with a shifted mean, $\hat{w}_\gamma \sim \mathcal{N}(\gamma, I)$. The β -term pushes the next state towards the representative point of the grid cell. Based on [42], we choose stochastic kernels $\bar{\mathcal{W}}_{ij}$ such that the probability of event $w - \hat{w}_\gamma = 0$ is large. The error dynamics conditioned on this event equal $x_\Delta^+ = Ax_\Delta(t) + B_w \gamma_{ij}(t) - \beta(t)$, where state x_Δ and state update x_Δ^+ are the abbreviations

of $x_\Delta(k) := x(t) - \hat{x}(t)$ and $x_\Delta(t+1)$, respectively. This can be seen as a system with state x_Δ , constrained input γ_{ij} , and bounded disturbance β .

For a given deviation δ_{ij} , we compute a bound on the allowable shift as $\gamma_{ij} \in \Gamma_{ij} := \{\gamma_{ij} \in \mathbb{R}^{n_w} \mid \|\gamma_{ij}\| \leq r_{ij}\}$ and we parameterize the shift $\gamma_{ij} = F_{ij}x_\Delta$ with the matrix F_{ij} . In the exact same fashion as the proof of Theorem 9 in [42], we can show that if there exists λ_{ij} and F_{ij} such that the matrix inequalities in (A.5) are satisfied, then the following implications also hold

$$\begin{aligned} x_\Delta^\top D x_\Delta \leq \epsilon_i^2 &\implies x_\Delta^\top F_{ij}^\top F_{ij} x_\Delta \leq r_{ij}^2 && (\text{input bound}) \\ x_\Delta^\top D x_\Delta \leq \epsilon_i^2 &\implies (x_\Delta^+)^\top D x_\Delta^+ \leq \alpha_{ij}^2 \epsilon_i^2. && (\text{contraction}) \end{aligned}$$

Therefore, we satisfy the bound $\gamma_{ij} \in \Gamma_{ij}$ and the simulation relation \mathcal{R}_i describes an α_{ij} -contractive set. Hence, using Lemma 6 in [42], we can conclude that there exists a kernel \bar{W}_{ij} , such that condition 2 in Definition 4.2 is satisfied. Since condition 1 in Definition 4.2 is already satisfied by choosing D appropriately, $\hat{\mathbf{M}} \preceq_\epsilon^\delta \mathbf{M}$ holds as long as the conditions in Theorem A.2 are satisfied.

Concluding, since (A.4) holds, condition 1 in Definition 4.2 is satisfied for all i, j . If in addition λ_{ij} and F_{ij} satisfy (A.5), then there exists a kernel \bar{W}_{ij} such that condition 2 in Definition 4.2 holds (Lemma A.1). Once this does not only hold for a specific i, j , but for all $i, j \in [1, \dots, N_R]$ and there exists $i \in \{1, 2, \dots, N_R\}$ with $(\hat{x}_0, x_0) \in \mathcal{R}_i$, then we have $\hat{\mathbf{M}} \preceq_\epsilon^\delta \mathbf{M}$. \square

Appendix B. Derivation for the ellipsoidal set of the waypoint model.

We want to find ϵ_w , or equivalently the ellipsoidal set \mathcal{E} as in (3.5), such that for all states corresponding to the ellipsoid around the waypoint, the next states remain inside the ellipsoid of the next waypoint, with a probability of $\Delta_w(x_w, x'_w)$. Mathematically, this can be formulated as follows:

$$\forall x \in \mathcal{E}(x_w), \forall u_w \in \mathbb{U}_w : x' \in \mathcal{E}(x'_w),$$

with probability $1 - \Delta_w(x_w, x'_w)$. This is equivalent to

$$(B.1) \quad \forall x \in \mathcal{E}(x_w), \forall u_w \in \mathbb{U}_w :$$

$$(B.2) \quad \|x' - x'_w\|_{D_w} = \|\bar{A}(x - x_w) + B_w u_w\|_{D_w} \leq \epsilon_w,$$

with $\bar{A} = A + BK$. Here, the interface function $u = u_w + K(x - x_w)$ has been substituted. Using standard properties of the vector norm [6, Chapter 1], we find the following inequalities

$$\begin{aligned} \|\bar{A}(x - x_w) + B_w u_w\|_{D_w} &\leq \|\bar{A}(x - x_w)\|_{D_w} + \|B_w u_w\|_{D_w} \\ &\leq \|\bar{A}\|_{D_w} \|(x - x_w)\|_{D_w} + \|B_w\|_{D_w} \|u_w\|_{D_w}. \end{aligned}$$

For all states $x_w \in \mathcal{E}(x_w)$ this implies that

$$(B.3) \quad \|x' - x'_w\|_{D_w} \leq \|\bar{A}\|_{D_w} \epsilon_p + \|B_w\|_{D_w} \|u_w\|_{D_w}.$$

For a given probability $\Delta_w(x_w, x'_w)$ and weighting matrix $D_w = d_w I_{n_x}$, with scalar d_w , we can compute a bound on w using the Chi-squared distribution with n_w degrees of freedom [13]. Hence, we obtain

$$(B.4) \quad \|w\|_{D_w} \leq \frac{1}{d_w} \sqrt{r_w}, \quad \text{with } r_w = \chi^{-1}(\Delta_w(x_w, x'_w) | n_w),$$

with $\chi^{-1}(\cdot|n_w)$ denoting the inverse cumulative distribution function of the Chi-squared distribution with n_w degrees of freedom. Intuitively, this means that for a random variable $w \sim \mathcal{N}(0, I)$, we compute the ellipsoidal set (B.4) containing w with a confidence equal to $\Delta_w(x_w, x'_w)$. Substituting in (B.3), we get

$$\|x' - x'_w\|_{D_w} \leq \|\bar{A}\|_{D_w} \epsilon_p + \|B_w\|_{D_w} \frac{1}{d_p} \sqrt{r_w}.$$

Hence, to achieve (B.1) ϵ_w should equal

$$(B.5) \quad \epsilon_w = | - (\|\bar{A}\|_{D_w} - 1)^{-1} \|B_w\|_{D_w} \frac{1}{d_w} \sqrt{r_w} |.$$